

# We are IntechOpen, the world's leading publisher of Open Access books Built by scientists, for scientists

6,900

Open access books available

186,000

International authors and editors

200M

Downloads

Our authors are among the

154

Countries delivered to

TOP 1%

most cited scientists

12.2%

Contributors from top 500 universities



WEB OF SCIENCE™

Selection of our books indexed in the Book Citation Index  
in Web of Science™ Core Collection (BKCI)

Interested in publishing with us?  
Contact [book.department@intechopen.com](mailto:book.department@intechopen.com)

Numbers displayed above are based on latest data collected.  
For more information visit [www.intechopen.com](http://www.intechopen.com)



# Adaptive Composite Materials: Bionics Principles, Abnormal Elasticity, Moving Interfaces

Shilko Serge

*V.A. Belyi Metal-Polymer Research Institute of NASB,  
Belarus*

## 1. Introduction

Requirements imposed on artificial materials are constantly rising with time. Along with lately requisite properties, including stability of physical and mechanical characteristics, linearity of the equation of state and unambiguity of response to disturbance, there arose a problem of a complex active response to varying outer conditions. In other words, a tendency is observed of increasing number of material functions acquiring the features of intellectual systems.

So, obvious prototypes of these materials turn to be biosystems, from the one hand, and computer monitored technical systems able to reproduce intellectual behavior using sensor, processor and executive functions (including effector function and response action), from the other hand, plus feedforward and feedback. Although means of these properties realization can't be similar in artificial materials and above mentioned natural prototypes, generalizations obtained at the junction of the materials science, bionics and cybernetics allow to formulate the conceptual principles and to consider probable ways of the named interdisciplinary problem solution.

Recent reviews and terminological discussions in the field have confirmed actuality of the structural and functional analyses of smart composites, including functional nanomaterials [Bergman & Inan, 2004]. However papers, devoted to such materials (e.g., self-controlled membranes on hydrogel base [Galaev, 1995]) are commonly reduced to creation of sensors and actuators. Less attention have received principles and models of adaptive reactions in composites. The adaptive mode of reinforcing and self-assembling in smart materials [Schwartz, 2007] has been studied below in the form of phenomena caused unusual elastic properties of auxetic and multimodule materials. The development of adaptive composites allows us to hamper the failure process and promotes reliability and service life of products for different technical applications.

## 2. Adaptive composites in classification of materials

### 2.1 Classification of materials

The first stage of the present study is classification of materials with account of interrelations found between structure and functions as well as analysis and modeling of a subclass of

intellectual systems, namely adaptive composite materials (ACM). Some of the assumptions put forward by the authors are based on the theory of functional systems and synergism [Prigogine & Stengers, 1984]. Three generations of materials which can be discriminated in the proposed classification, are given in Table 1.

Generation of materials	Structural-and-functional characteristics	Means of property regulation	Factor determining optimum result
Traditional material	Monofunctional single-component material	Properties determined a priori by the origin of component material	Initial property of monocomponent
Composite material	Monofunctional polycomponental material with fixed boundaries between components	Properties are efficiently regulated technologically based on principles of additivity and synergism	Initial property of components and intermediate layers
Smart (adaptive) composites	Polyfunctional polycomponental material with movable boundaries between components	Self-regulation of structure based on sensor, processor and effector functions and feedforward and feedback channels	Efficiency of sensing extreme effects and elimination of refusals

Table 1. Evolution of structure and properties of materials

The first generation is traditional materials including monofunctional medium whose properties are determined by the nature and initial quality of a single component. The next are traditional composites with a prominent structural hierarchy, being also monofunctional. They are characterized by stability of inner and external boundaries, i.e. fixed structure of components, intermediate layers and the composite as a whole. Adaptive materials with coordinated functions and active behavior belong to the third advanced generation of materials. These systems perceive outer effects at unchanged function owing to, presumably, structural self-organization. In this connection, the mobility of the component boundaries should be remembered as an indispensable property of smart materials, which is not present in traditional composites.

The qualitative transition of materials from the passive to active functioning is shown in Table 2. Naturally, prerequisites of such a transition are formed at the levels of two preceding generations. Thus, transformation of one physical field into another (e.g., piezo- or photo effects) is probable at the stage of monofunctional material. The creation of qualitatively new (emerged), including forecast properties, is a logical continuation of the additive and synergetic principles of composite production. This precedes the development of adaptive composites, being a subclass of smart systems with the dominating adaptive strategy.

The suggested classification makes it possible to forecast other unknown materials of the intellectual type, for example, capable of self-destruction “kamikaze”, those ensuring partial or full restoration “regenerators” and materials offering programmed control of the environment (“cyber”) and implicit (“incognito”) ones. These subclasses constitute a new type of “ecophilous” materials which behavior supports homeostasis of the environment.

Functional evolution	Degree of activity	Degree of intellect	Functioning quality	Mode of behavior
mono-functional	passive	“trivial”	material	“predictable”
	active	“wit” (functional)		
poly-functional	active	smart (adaptive)	material = part	“indefinite”
				“egoist”
			material = system	“time-server”
		“wise” (ecophilous)	material = medium	“kamikaze”
				“regenerate”
				“cyber”
				“incognito”

Table 2. Systematization of materials by general criteria

2.2 Adaptive composites

Relative simplicity of ACM is due to their orientation aimed to fulfill only the adaptive function of the part or a system in contrast to a higher status of the material-medium subclass (Table 2). However the adaptive composite is formed rather in time than by a mechanical mixing of structural components, and evolutionizes as a specific unit by coordinating interrelated physical processes based on an imparted optimum criterion. In this case, the emergence of macrostructure is specified by origination of collective modes under the action of fluctuations, there competing and, finally, by selection of the most accommodated mode or their combination [Prigogine & Stengers, 1984]. The structures themselves could be described in physical terms as types of adaptation to outer conditions.

2.2.1 Self-organization of material structure

Reaction of a material due to mutual coordination of structural and functional parameters of microsystems characterizes it as an open self-regulating system. Selection of the mode of

behavior in response to outer effect does not arise from the principle of the least action, neither from the principle of compulsion (Gauss principle) nor from that of the utmost probability. Active response systems eliminate (or subordinate) contingency. This makes grounds to speak about a programmed behavior of the system, i.e. the decision is made according to the inner criteria determined by the structure itself and system parameters, which substantiates the necessity of direct and reverse connection channels.

It follows from the above said that to form a more complex processor function of ACM it is possible to use the universe phenomenon of self-organization, which is not limited to only systems of higher organization and functional complexity and isn't a monopoly of bio- or social systems. A self-organizing system is understood as a system capable of stabilizing parameters under varying outer conditions through directed ordering of its structural and functional relations aimed at withstanding entropic factors of the environment, which helps to preserve its characteristics as an integral formation [Prigogine & Stengers, 1984].

The material formed by combining its components acquires the characteristics of a composite structure, which is a notion nonequivalent to the structure of its constituents. This fact raises composite materials to a higher structural level and admits the probability of per layer differentiation of the functions in order to reach the integral control system. In our view, to realize adaptation mechanism to outer conditions in composite materials, it's worthwhile considering the combination of different scale physical processes, where we single out at least 4 structural levels: molecular, mesoscopic, macroscopic and polycomponental (Figure 1).

The molecular level is the basic one at programming material behavior. This is because its scale in polymer composites corresponds to cooperative effects of segmental mobility and conformational rebuilding that provide conditions for self-organization in high-molecular bodies. Just here the processor function is realized as a capacity for estimating variations due to outer effects and as a tool formulating the character and force of response based on stationary characteristics of the microsystem. Also, the effector function is fulfilled here for exciting reverse reactions by varying characteristics of the microsystem on a self-organization base.

The mesoscopic level performs the sensor function as an ability to perceive outer effects. Non-equilibrium processes are initiated at this level changing molecular structure and supporting the interaction of direct and reverse channels between the levels.

The macroscopic level makes provision for the mobile function as a reorganization of the initial subsystems (components) aimed at preserving the behavior model.

The mobile function is also realized at the polycomponental level, though intention in this case is to provide the system (material = article) functioning as a whole.

To organize control, the processes relating to the mentioned levels should be coordinated using functional links between them.

It is to be remembered that polymer composites are potential carriers of intellectual properties. Namely, they are sensitive to physical fields, i.e. show a sensor function; make it possible to carry out the actuator function (shape memory of thermosetting resins, etc) and, finally, among all other artificial material media they most closely approach the living nature (biotissues are usually built of high-molecular compounds).

The study of synergetic phenomena in nonliving nature as a linking element between analogous processes in original objects will, in our opinion, provide a possibility to find structural-and-functional bioprototypes of adaptive composites.

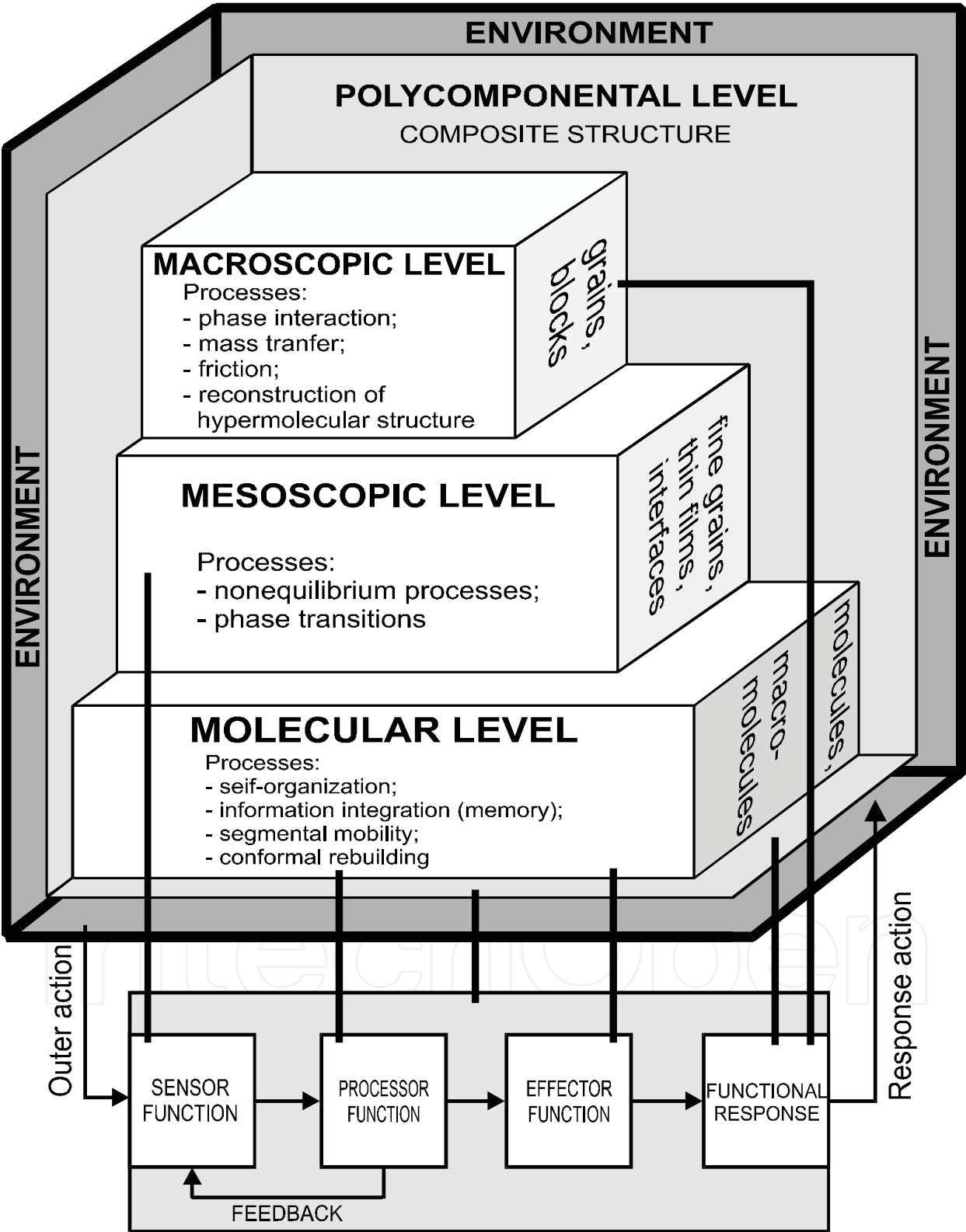


Fig. 1. Differentiation of structural levels at ACM development



### 3. Self-reinforcing in auxetic composites

The effort towards improving the performance of novel devices based upon realisation of non-linear and non-trivial (anomalous) deformation properties of materials is the aim of many current investigations. First, we shall consider the materials with a negative Poisson's ratio,  $\nu$ , termed 'auxetics'. Data structuring, examination of the mechanisms of generating the negative Poisson's ratio and analysis of likely applications for auxetics have been discussed recently in [Wojciechowski et al, 2007] and reviewed particularly in [Koniok et al, 2004]. Poisson's ratio affects a very important mechanical property, i.e. compressibility of a material. Under a uniaxial stress, auxetics expand/contract at the direction perpendicular to the tension/compression direction, respectively as shown in Figure 2.

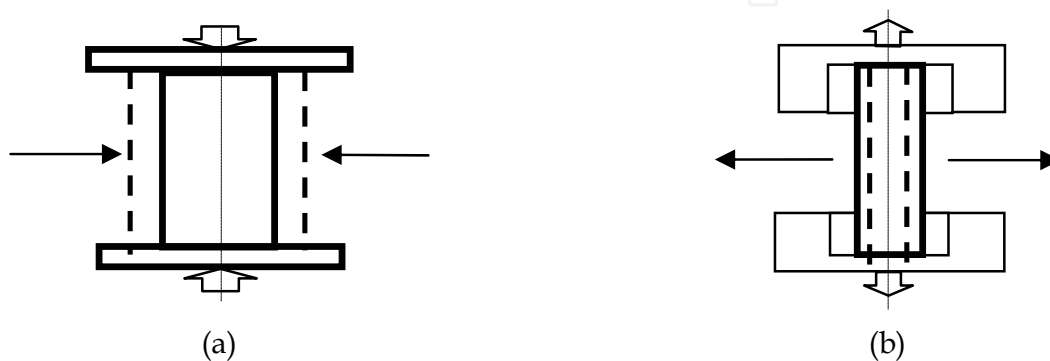


Fig. 2. The deformation mode of an auxetic material under uniaxial stress: (a) compression, (b) tension. Initial configuration before loading has been shown by dashed lines

This property should influence stiffness and slip under contact loading, and in this way allow control over deformability and friction characteristics of composites and joints based on auxetics. As will be shown, the contact characteristics vary dramatically with variation of the sign of Poisson's ratio. In the classical elasticity theory for isotropic bodies [Landau & Lifshitz, 1986] Poisson's ratio  $\nu = (3K - 2\mu) / (6K + 2\mu)$ , where  $\mu$ ,  $K$  are the shear and volume moduli respectively, the Poisson's ratio of isotropic bodies can vary in the limits  $-1 \leq \nu \leq 0.5$ . The upper limit corresponds to incompressible materials, e.g. rubber, whose volume remains constant at significant shape variations, the lower one belongs to the materials preserving their geometrical form with changing volume.

Several natural and artificial auxetic materials have been described to date, but experimental and theoretical studies of the adaptive frictional and mechanical properties of these materials are not still well developed [Baughman & Galvao, 1993]. For example, there exists the possibility for realisation of self-reinforcing or self-locking effect in contact joints containing auxetic components. As a result, this effect would bring about a significant increase in the bearing capacity of frictional joints or shear strength of the fibre - matrix interface under mechanical or thermo-mechanical load.

Of specific interest here is the study of the self-locking effect under contact deformation of anisotropic auxetics based on directionally reinforced composites. This is because such materials may possess Poisson's ratios of much less than -1 ( $\nu < -50$ ) and considerable strength due to their directional reinforcement.

The approaches available for creation of composites with  $\nu < 0$  assume either the use of individual auxetic components or formation of an auxetic composite - a combination of

structural units of mesoscopic level (pores, granules, permolecular formations of polymers, etc). To study friction effects under contact loading the existing estimates of elastic properties of quasi-isotropic and anisotropic composites should be taken into account.

3.1 Auxetic inclusions (quasi-isotropic auxetics)

In [Wei & Edwards, 1999] the mechanical characteristics of a composite with ellipsoidal and spherical particles were calculated for the case of randomly distributed filler particles. Simulation results under different ratios of filler stiffness to matrix stiffness, for 45% volume fraction, are presented in Table 3.

Inclusion geometry	0.1	1.0	10
Disc (2D)	-0.3020	-0.2856	0.1216
Disc (3D)	-0.0385	-0.3575	-0.7387
Sphere	-0.0624	-0.2081	0.0650
Wedge (2D)	-0.2679	-0.2266	-0.0508
Needle (3D)	-0.0555	-0.1714	-0.0562

Table 3. Effective Poisson’s ratio  $\nu_c$  of the composite at  $\nu = 0$

The possibility of obtaining auxetic composites using filled polymers has been considered in [Kolupaev et al, 1996]. The authors have obtained such composites using thermoplastic polyurethane with ultra-dispersed (0.3-1  $\mu\text{m}$ ) particles of tungsten, iron and molybdenum having  $\nu \approx -0.2-0.4$ . The composite possessed auxetic properties due to internal stresses  $\sigma_{in}$  produced by the inclusions in the matrix in the range  $0.97 \text{ MPa} < \sigma_{in} < 7.11 \text{ MPa}$ .

3.2 Non-auxetic inclusions (anisotropic auxetics)

Let us consider a composite formed by the oblique packing of fibres in an elastic incompressible elastomeric matrix (Figure 3a).

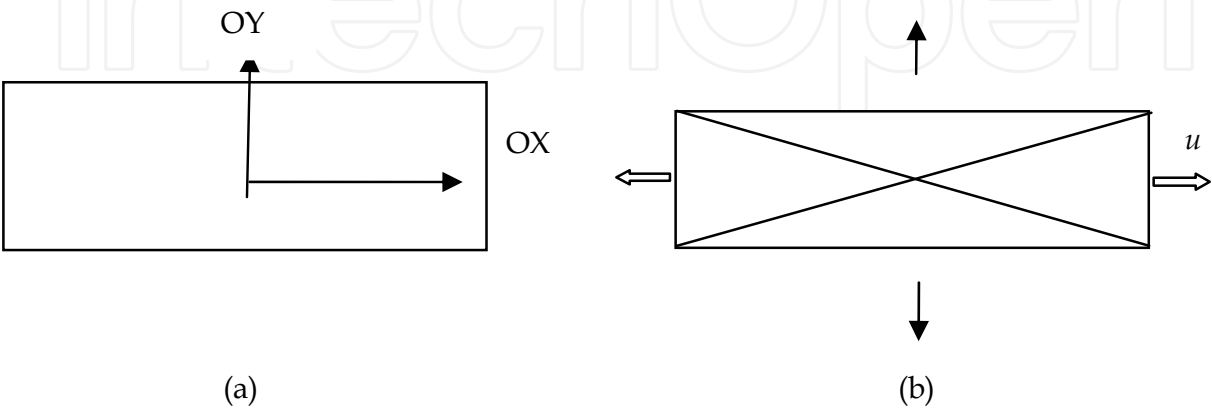


Fig. 3. Structure (a) and the mesofragment (b) of obliquely reinforced auxetic composite



At  $E_2 \ll E_1$  we get  $\nu_{xz} \approx 1 - \text{ctg}^2 \theta$ , where  $E_1, E_2$  are Young's moduli of the fibres and matrix respectively. For small fibre packing angles,  $\theta$ , Poisson's ratio  $\nu_{xz}$  has negative values. The deformation results in a pantographic change in orientation of the fibres, which elongate insignificantly compared to the low-modulus matrix, thus promoting its contraction normal to the reinforcement direction. To this class of auxetics belong the laminates produced by the oblique superposing of the layers (Figure 3b). Investigations into laminates made of prepreps with carbon fibres and epoxy matrix have shown that  $\nu_{xz}$  of the composite obtained at small packing angles of the layers ( $10^\circ$ - $40^\circ$ ) is negative.

### 3.3 Analysis of contact deformation of auxetic composites

The stress state parameters were determined for the double-lap type joint in conditions of initial compression  $\delta_y$  and compression with shear  $\delta_x$  (Figure 4a). The analysis of the auxetic element 1 interaction with two conjugated and located symmetrically non-deformable bodies 2 and 3 (Figure 4b) has been carried out using the finite element solution of contact problem with friction.

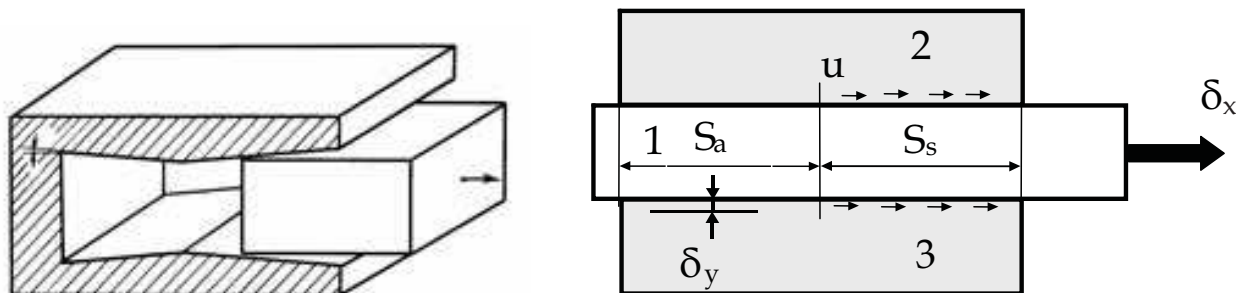


Fig. 4. General view (a) and calculation scheme (b) of a frictional joint with auxetic element

A peculiarity of this problem is a considerable nonlinear deformation brought about in conditions of unlimited shear by formation of the zones of adhesion  $S_a$  and slippage  $S_s$  with nonzero tangential contact displacements  $u$  (Figure 4b). Under compression of the joint the slippage zones are located symmetrically to the central zone of adhesion. Shear application leads to violations of this symmetry. The limiting load capacity of the joint is dependent on slippage onset over the whole contact area which, in its turn, is dependent upon the material compressibility.

For the case of a quasi-isotropic material Poisson's ratio was varied within theoretically acceptable values of the isotropic elastic medium, i.e.  $-1 \leq \nu \leq 0,5$ . The extreme values of the contact stresses tend to localise near to the right edge of the junction. The contact parameters vary insignificantly for the positive Poisson's ratios typical of isotropic materials, except for the limiting values characteristic for practically incompressible elastomers. Incompressibility ( $\nu = 0.48$ - $0.5$ ) results in the elastic compression of the material and contact slippage. The stress strain state parameters including the maximal equivalent stress  $\sigma_{eqv}$ , contact pressure  $p$ , tangential stress  $\tau$  and slippage  $u$ , have been studied as a function of Poisson's ratio for the quasi-isotropic materials and the reinforcement angle for the anisotropic ones (Figure 5). An abrupt leap in the maximal contact parameters is observed when  $\nu < 0$ , not seen with the positive Poisson's ratios. This increase is most marked when  $\nu < -0.9$ . The adaptive mode of friction has been studied in the form of a self-locking effect under contact loading in

isotropic and anisotropic auxetic cases [Shilko et al., 2008a]. This effect suggests that the strength of such a joint rises with increasing shear load.

Similar calculations have been made for a joint with a deformable element of the anisotropic auxetic composite on the low-modular matrix base (see section 3.2, Fig. 3) under varying reinforcement angles that determine the elastic moduli  $E_x, E_y, E_z, \nu_{xy}, \nu_{yz}, \nu_{xz}, G_{xy}, G_{yz}, G_{xz}$ . These elastic constants (Table 4) were calculated based on the volume fraction of the fibrous filler with  $\mu = 0.1$ , elasticity modulus and Poisson's ratio of the matrix and filler, respectively  $E_m = 4 \text{ MPa}$ ,  $\nu_m = 0.5$ ,  $E_f = 1.5 \text{ GPa}$ ,  $\nu_f = 0.4$  using the formulas

$$\begin{aligned} E_x &= \frac{1}{a_{11}}; E_y = \frac{1}{a_{22}}; E_z = \frac{1}{a_{33}}; G_{xy} = \frac{1}{a_{66}}; G_{yz} = \frac{1}{a_{55}}; G_{xz} = \frac{1}{a_{44}}; \\ \nu_{xy} &= -E_x a_{12}; \nu_{yz} = -E_y a_{23}; \nu_{xz} = -E_x a_{13}. \end{aligned} \quad (1)$$

where  $a_{ij}$  are compliance coefficients of a unidirectional composite:

$$\begin{aligned} a_{11} &= \frac{1}{(1+(n-1)\mu)E_m}, \quad a_{22} = a_{33} = \frac{\left(\mu + n(1-\mu)(1+(n-1)\mu) - (n\nu_m - \nu_f)^2 \mu(1-\mu)\right)}{(1+(n-1)\mu)E_f}, \\ a_{12} &= a_{13} = -\frac{\nu_m(1-\mu) + \nu_f \mu}{(1+(n-1)\mu)E_m}, \quad a_{23} = -\frac{(\nu_f \mu + n\nu_m(1-\mu))(1+(n-1)\mu) + (n\nu_m - \nu_f)^2 \mu(1-\mu)}{(1+(n-1)\mu)E_f}, \\ a_{66} &= a_{55} = 2 \frac{(1+\nu_m)(n(1+\nu_m)(1-\mu) + (1+\nu_f)(1+\mu))}{(n(1+\nu_m)(1+\mu) + (1+\nu_f)(1-\mu))E_m}, \quad a_{44} = 2 \frac{(1+\nu_f)\mu + n(1+\nu_m)(1-\mu)}{E_f} \end{aligned} \quad (2)$$

where  $n = E_f / E_m$ .

The minimal Poisson's ratio  $\nu_{xz} = -2.142$  is attained when the angle between the reinforcement direction and OY axis is  $70^\circ$  and deformation  $u$  is directed along OX axis (Figure 3).

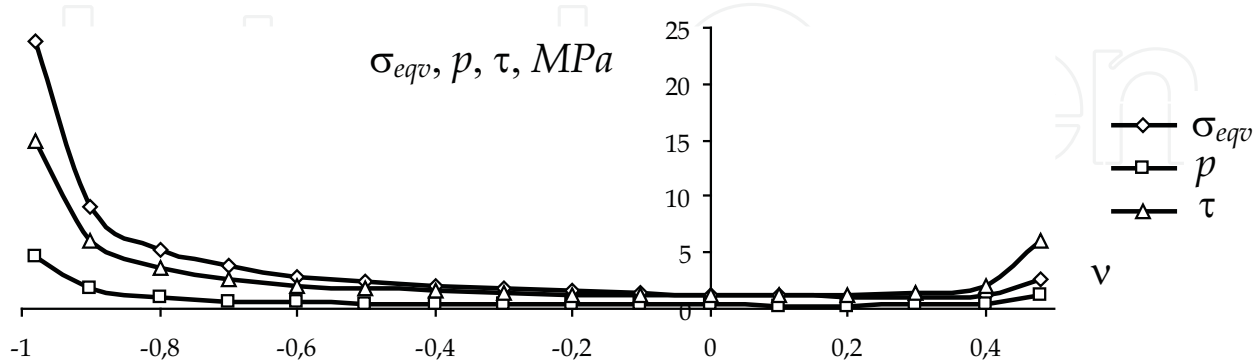


Fig. 5. Maximal values of equivalent stresses, contact pressures and tangential stresses as dependent on Poisson's ratio

The maximal contact parameters were determined for different surface geometries of the conjugated bodies, namely plane, cylindrical (curvature radius  $r = 100 \text{ mm}$ ) and wedge-like

(wedge aperture angle  $\alpha = 174^\circ$ ). It is seen in Figs. 6-10 that the extreme dependence of contact stresses is characteristic for all geometries with a minimum at reinforcement angle  $45^\circ$ .

$\varphi$ , degree	0	15	30	45	60	70	80	90
$E_x$ , MPa	6.627	6.286	5.619	7.788	38.47	133.4	266.8	303.2
$E_y$ , MPa	303.2	207.5	38.47	7.788	5.619	6.051	6.471	6.627
$E_z$ , MPa	6.627	7.259	11.96	81.50	11.96	7.95	6.88	6.627
$v_{xy}$	0.010	0.082	0.336	0.945	2.242	2.793	0.912	-0.48
$v_{yz}$	0.480	-1.727	-1.316	0.048	0.662	0.858	0.958	0.989
$v_{xz}$	0.989	0.918	0.662	0.048	-1.316	-2.142	-0.743	0.48
$G_{xy}$ , MPa	1.996	21.1	59.58	78.17	63.31	42.49	16.98	1.996
$G_{yz}$ , MPa	1.996	2.285	3.181	3.754	2.753	2.521	1.771	1.666
$G_{xz}$ , MPa	1.666	1.910	2.753	3.754	3.181	2.117	2.122	1.996

Table 4. Elastic constants for obliquely reinforced composite as a function of reinforcement angle  $\varphi$

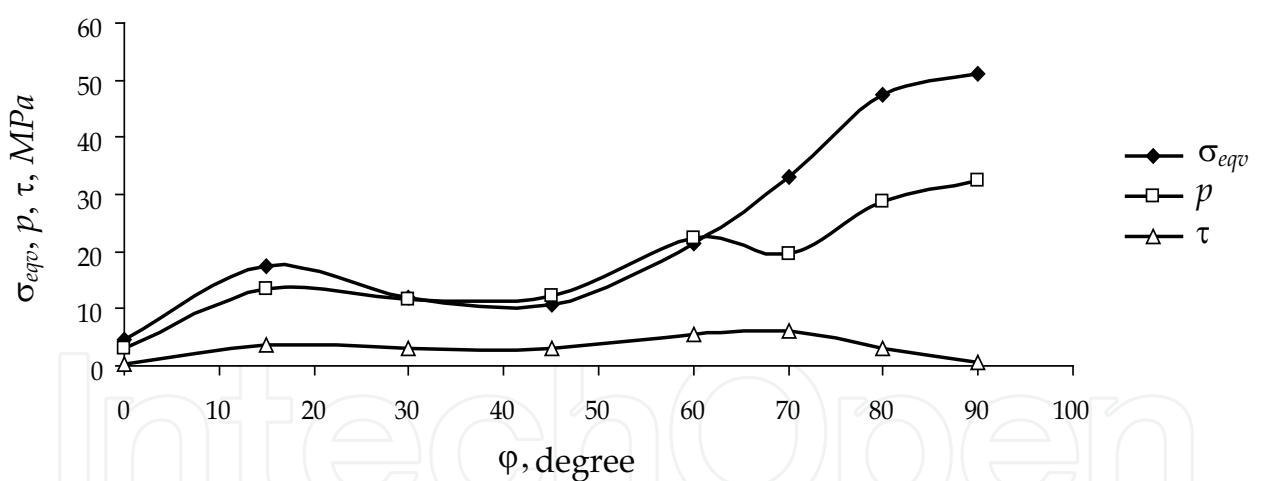


Fig. 6. Dependence of maximal values of equivalent stress, contact pressure and tangential stress on reinforcement angle at compression:  $\delta_y = -1$  mm (plane surface)

With a plane surface of the conjugated bodies (Figures 6, 7) the dependencies of stresses  $\sigma_{eqv}(\varphi)$ ,  $p(\varphi)$ ,  $\tau(\varphi)$  have local maxima. Their location varies with increasing shear due to slipping.

For cylindrical conjugated bodies, the local minima are absent under pure compression of the auxetic section, although shear promotes their appearance in the region of large reinforcement angles (Figures 8, 9).

It is peculiar that the auxetic body in a junction with a wedge surface shows a rather weak shear effect upon the contact stress state. Similarly to the case of planar surfaces, the local

minima of maximal stress  $\sigma_{eqv}$  and contact pressure  $p$  correspond to the reinforcement angle of  $\varphi = 15^\circ$ .

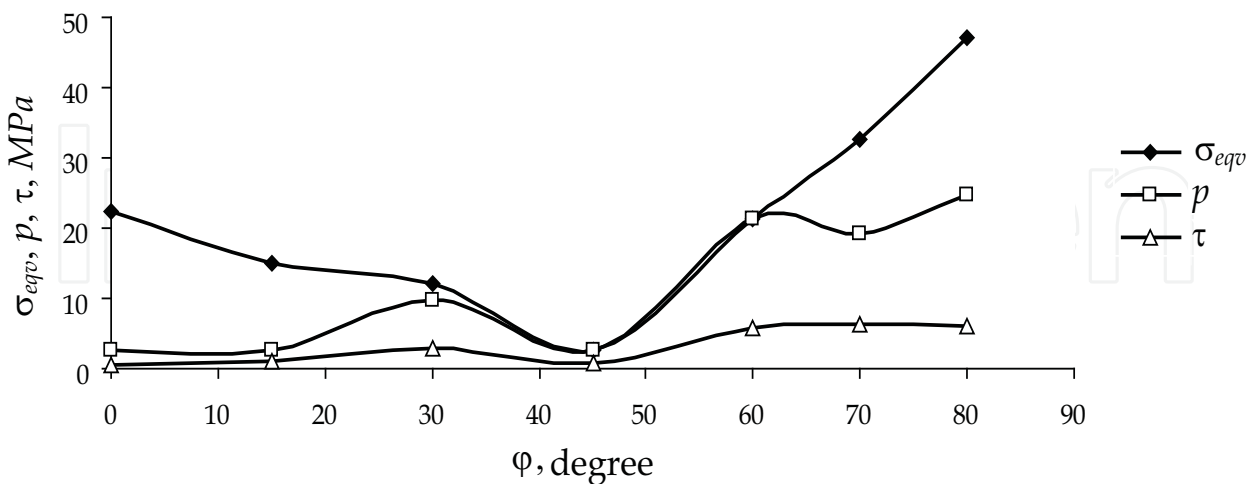


Fig. 7. Dependence of maximal values of equivalent stress, contact pressure and tangential stress on reinforcement angle at compression with shear:  $\delta_y = -1$  mm,  $\delta_x = 5$  mm (plane surface)

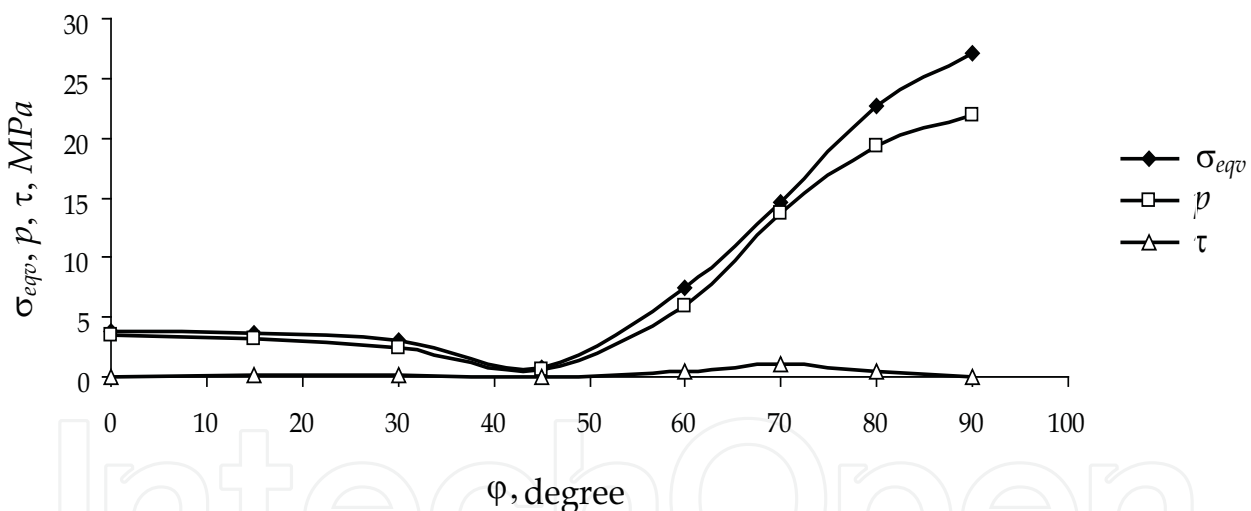


Fig. 8. Dependence of maximal values of equivalent stress, contact pressure and tangential stress on reinforcement angle at compression:  $\delta_y = -1$  mm (cylindrical surface)

So, promising functional materials with negative Poisson’s ratios (auxetics) have been considered. The results reported here help to quantitatively evaluate the influence of Poisson’s ratio (in the isotropic materials) and reinforcing angle (in the anisotropic composites) for compression and compression with shear contact interactions. The adaptive mode of friction has been studied in the form of self-reinforcing under contact loading in isotropic and anisotropic auxetics. This effect suggests that the bearing capacity of such a frictional joint rises with increasing shear [Shilko & Stolyarov, 1996]. It is shown that the use of auxetic materials is an efficient means of improving the mechanical and frictional characteristics of composites.

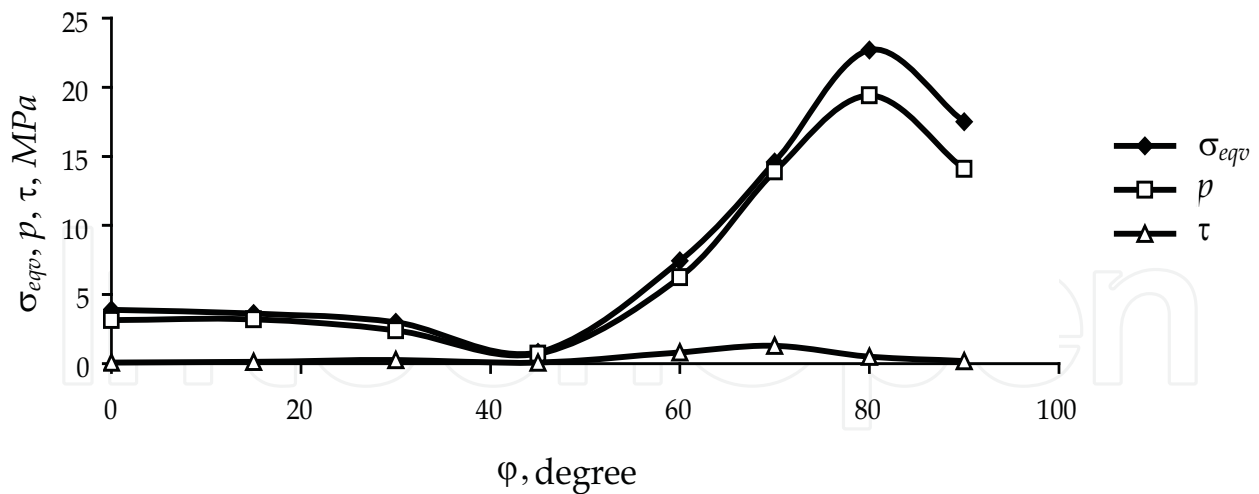


Fig. 9. Dependence of maximal values of equivalent stress, contact pressure and tangential stress on reinforcement angle at compression with shear:  $\delta_y = -1$  mm,  $\delta_x = 0.1$  mm (cylindrical surface)

#### 4. Self-structuring of multimodule materials

As it was mentioned above, in contrast to traditional composites, which display stable interfaces between components determining invariability of technologically specified complex of properties (Table 1), the adaptive material admits mobility of interfaces.

As a consequence, description of able to regulate its structure ACM proceeding from the given optimal criterion presumes statement of the moving boundaries problem and use of methods for its solution. In this connection, let's turn to investigation results of elastic (reversible) remodelling of a physically nonlinear multimodular metals such as Fe, Al, Cu, Mg, etc [Bell, 1968] (particularly, in Figure 10 these data are given for Fe). Softening of bulk modulus near the volume phase transition has been observed in polymer gels too [Hirotsu, 1991]. In the paper [Baughman & Galvao, 1993] it has been shown that crystalline networks demonstrates unusual mechanical and thermal properties.

The hypothesis is to be introduced into the course of the model development according to which the adaptive reaction reduces is a specific transfer process to an optimum control over intrinsic to ACM moving boundaries.

Let a composite at the polycomponental level be formed by bonded elastic particles (Fig. 11a). Being initially homogeneous and isotropic, each particle is characterized under the force action by stress concentration in the contact zone with the neighboring particle (Fig. 11b). The role of the sensor function is presumed to be played by characteristic for a number of substances multimodule ability [Bell, 1968], that is, the presence of a set of  $n$  discrete values of Young's modulus  $E$  depending on stress  $\sigma$ , being in this case the control parameter. For numeric modeling of adaptation to extreme external loads, which are by far higher the acceptable one for the initial material, discretization of each particle by finite elements and block relaxation algorithm, are used. A system of inequalities is taken as a processor function of the multimodule composite, where the lower and upper estimates of stresses are corrected at model "exposure" proceeding from the optimum criterion, namely, the condition of the minimal equivalent stress  $\sigma_{eq}$

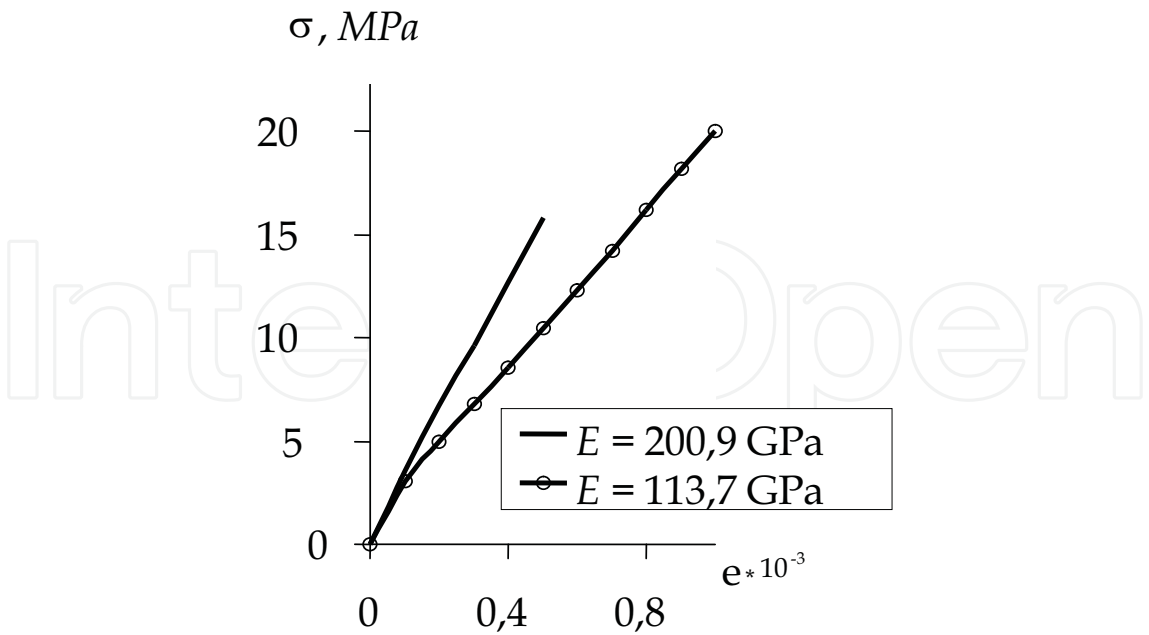


Fig. 10. Stress–strain curve of multimodule material (Fe) having two values of elastic modulus  $E$

$$E = \begin{cases} E_1, & \text{if } \sigma^0 \leq \sigma \leq \sigma^1; \\ \text{-----} \\ E_l, & \text{if } \sigma^{l-1} \leq \sigma \leq \sigma^l; \\ \text{-----} \\ E_n, & \text{if } \sigma^{n-1} \leq \sigma \leq \sigma^n, \end{cases} \tag{3}$$

Simulation results prove that the adaptive reaction consists in transformation of the initial homogeneous structure into a reversible inhomogeneous one (Fig. 11c,d) ensuring perception of extreme loads through effective reduction of stress concentration due to dynamically optimal distribution of elastic modulus  $E$ . So, the statement and systematic analysis of the problem of developing adaptive composites has enabled to trace evolution of structural organization of artificial materials, to clarify mechanisms of adaptation to external media and to disclose, to a certain degree, the effect of structure on formation of the optimum back reaction. In above considered example simulation of composite materials adaptivity is formulated as a problem on localizing moving internal boundaries, while differentiation of material functions is related to the changing scale level of the structure.

**5. Self-assembling of auxetic porous composites with multimodular solid phase**

Porous or cellular materials like «solid – gas» inhomogeneous systems are efficient composite structures in respect to optimizing strength and stiffness for a given weight.

These materials are useful for cushioning, insulating, damping, absorbing the kinetic energy from impact, packing, etc. Stiff and strong ones are preferable in load-bearing structures such as a lightweight core in sandwich panels. The term cellular is appropriate when the material contains polyhedral closed cells, as if it had resulted from solidification of a liquid foam.

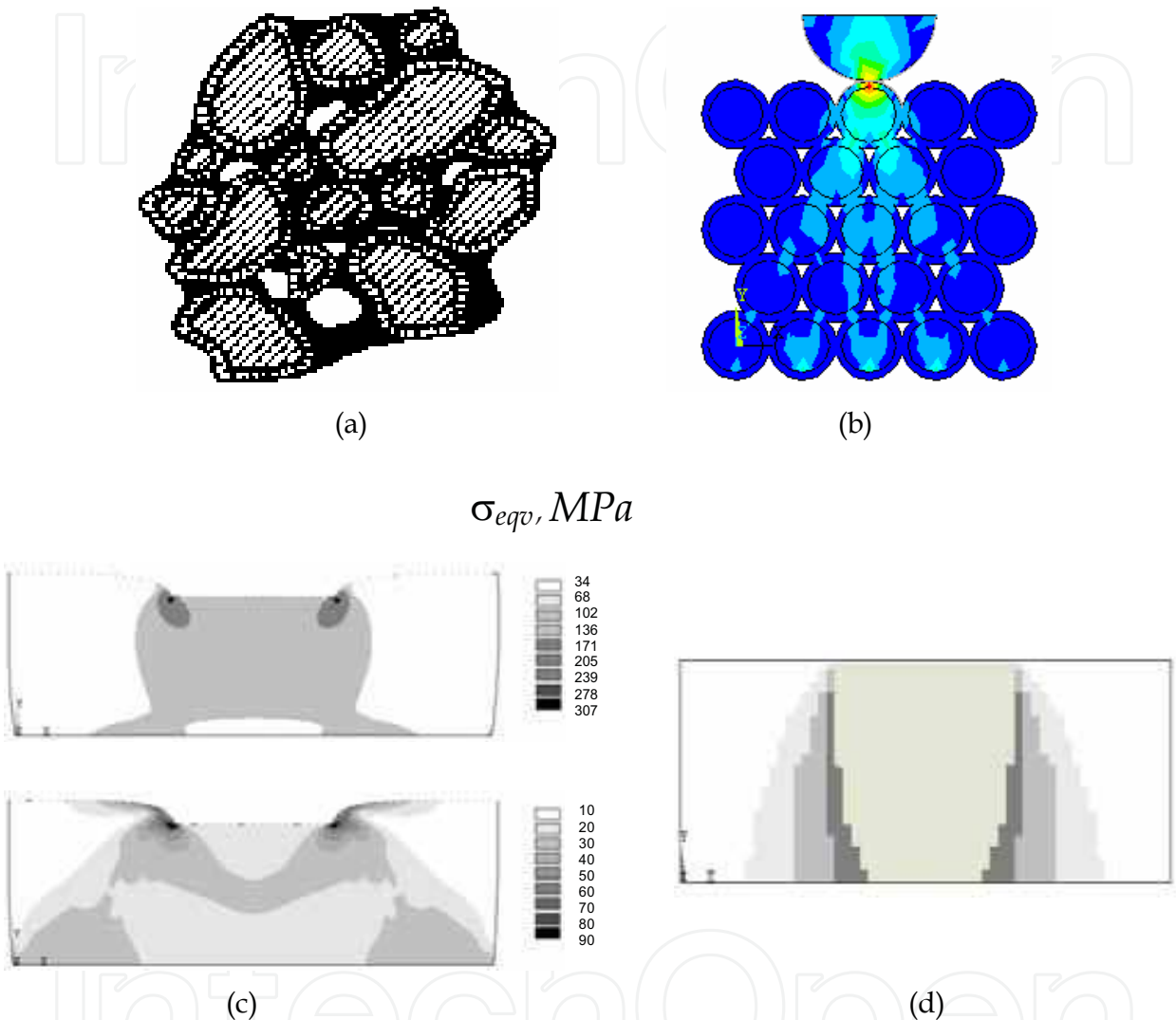


Fig. 11. ACM response after loading: typical composite structure (a); mesomechanical model (b); initial and final (after remodeling) distribution of equivalent stresses  $\sigma_{eq}$ . (c); dynamically optimal distribution of elastic modulus  $E$  (d)

A new means of improving the mechanical characteristics may be realized using abnormal deformation properties of auxetic porous materials having a negative Poisson's ratio  $\nu$  [Lakes, 1987]. Auxetic porous materials, including auxetic porous nanomaterials (APN), having very high mechanical properties, are suitable for creating adaptive contact joints and for replacing natural materials such as damaged bone and tooth biotissues. Examination of the mechanisms of generating a negative Poisson's ratio has been discussed and published in the last years, including special issues of *physica status solidi (b)* journal [Wojciechowski et al, 2007]. It is known that the inverted or re-entrant cell structure of



porous auxetics may be obtained by isotropic permanent volumetric compression of the conventional foam, resulting in non-reversible micro-buckling of the cell walls. There is interest in compression-driven self-assembly as a means to create auxetic porous structures at the nanoscale. Below we predict the deformation behaviour of porous materials under uniaxial tension and compression (by an analytical method) and contact compression (by the finite element method).

5.1 Analytical determination of porous material elastic modulus

For open-cell flexible cellular materials, Poisson’s ratio can be determined by a rod type structural unit with chaotically oriented cubic cells, as presented in Figure 12. It is worth mentioning that such a kind of unit cell model has been simulated in reference [Gibson & Ashby, 1982]. However, a cubic, not a spherical, structural unit had been used. Also, shear deformation of the rods had not been taken into account.

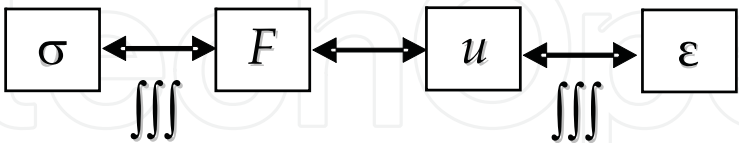
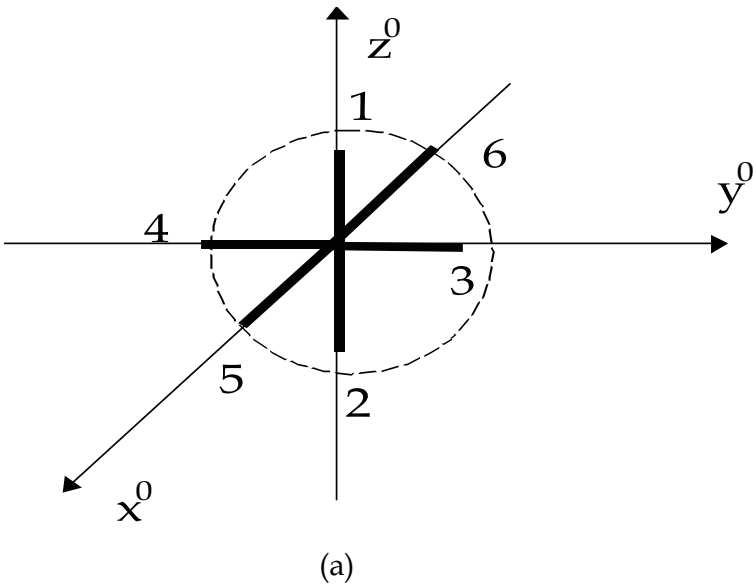


Fig. 12. Structural unit (a) and simulation procedure (b) of flexible cellular plastics:  $\sigma$ ,  $\epsilon$  are stress and strain tensor components;  $F$  is force acting on the rod end;  $u$  is displacement of force application point relatively to the rods;  $\overline{\phantom{x}}$  is averaged over direction

The rods of this structural unit are directed normally to the cubic planes. Symmetry of the element allows one to represent the displacement of the force application points (ends of rods) relatively to the rod joints through the deformation tensor components.

$$\begin{aligned}
\Delta x_{L1} &= x_{L1} - L = L\varepsilon_{z^0 z^0}, & y_{L1} &= \frac{L}{2}\sqrt{\gamma_{x^0 z^0}^2 + \gamma_{y^0 z^0}^2}, \\
\Delta x_{L3} &= x_{L3} - L = L\varepsilon_{y^0 y^0}, & y_{L3} &= \frac{L}{2}\sqrt{\gamma_{x^0 y^0}^2 + \gamma_{y^0 z^0}^2}, \\
\Delta x_{L5} &= x_{L5} - L = L\varepsilon_{x^0 x^0}, & y_{L5} &= \frac{L}{2}\sqrt{\gamma_{x^0 y^0}^2 + \gamma_{x^0 z^0}^2},
\end{aligned} \tag{4}$$

where  $L$  is the structural unit rod length;  $x_{Li}$ ,  $y_{Li}$  are the coordinates for the end of the  $i$ -th rod ( $i = 1..6$ ) in the  $xy$  coordinate system; the  $x$  axis is directed longitudinally to the  $i$ -th rod in the non-deformed state (Figure 13).

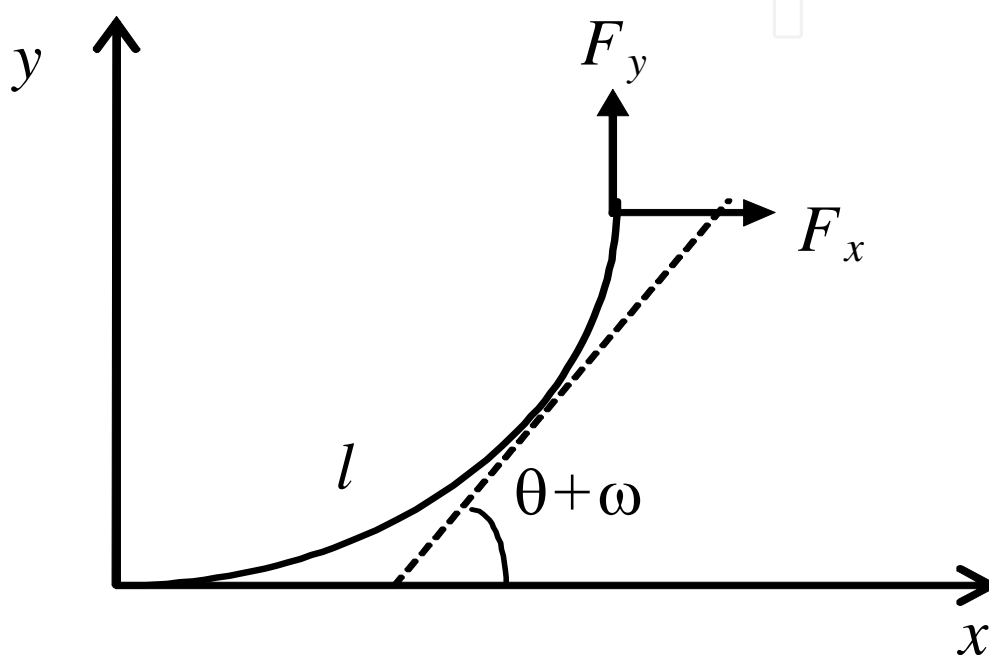


Fig. 13. Scheme of cantilever beam under large bending

Eq. (4) refers to deformations for which the Cauchy relations are satisfied. Here, the parameter  $L$  can be related to the solid state volumetric fraction by the following equation

$$V_f = \frac{V_m}{V} = \frac{9}{2\pi q^2}, \tag{5}$$

where  $V_m$  is the volume of rods in the structural unit;  $V$  is the structural unit total volume before deformation;  $q$  is the rod length  $L$  to its cross sectional side length  $r$  ratio. For simplification we neglected the volume of the nodes (rod joints) and assumed that the rods have a square cross-section. During further calculations we have estimated that the simulation results do not depend on the  $r$  value. So we may assume that  $r = 1$ ,  $L = q$ .

Let us assume that in the coordinate system  $XYZ$  uniaxial strain is defined as  $\varepsilon_{nn} = f(t)$  (other components of strain are equal to zero). The system  $XYZ$  position relative to the system  $x^0 y^0 z^0$  is defined by Euler's angles  $\beta_1$ ,  $\beta_2$ ,  $\beta_3$ . Once the function  $f(t)$  and Euler's angles are known, these define the deformation components in the  $x^0 y^0 z^0$  system (Fig. 12). Then, the displacements (4) can be written as follows:

$$y_{Li} = \varepsilon_{nm}(t)\eta_i(\beta_1, \beta_2, \beta_3), \quad \Delta x_{Li} = \varepsilon_{nm}(t)\xi_i(\beta_1, \beta_2, \beta_3). \quad (6)$$

Here  $\eta_i(\beta_1, \beta_2, \beta_3)$ ,  $\xi_i(\beta_1, \beta_2, \beta_3)$  are the Euler's angle functions which are related by recalculating the tensor components under coordinate axis rotation. For the determination of forces  $\vec{F}_i$  acting at the ends of the rods by the set deflections, it is necessary to solve a large flexure problem of a cantilever beam taking into account material viscosity. At the same time, to describe deformation of the low-density porous materials ( $V_f < 0.1$ ) it can be assumed that the rod is deformed equally over all length  $L$ . The viscoelastic behaviour of the rod material is described by Rzhanitsyn's relaxation function

$$R(t) = Ae^{-\beta t}t^{\alpha-1}, \quad (7)$$

where  $t$  is time,  $s$ ; and  $A$ ,  $\alpha$ ,  $\beta$  are the kernel parameters.

The stress/strain relations are determined by the following equation

$$s_{\rho\chi} = 2G_f \left( v_{\rho\chi} - \int_0^t R(t-\tau) v_{\rho\chi}(\tau) d\tau \right), \quad \sigma = 3K_f \varepsilon. \quad (8)$$

where  $s_{\rho\chi}$ ,  $v_{\rho\chi}$ ,  $\sigma$ ,  $\varepsilon$  are the deviatoric and spherical parts of the stress and strain tensors;  $G_f$ ,  $K_f$  are the shear and bulk moduli of the material.

For the beam deformations, let us assume

$$\varepsilon_{ll} = \varepsilon_0(l) + \lambda \theta'(l), \quad \varepsilon_{\lambda l} = \frac{1}{2} \omega(l). \quad (9)$$

where  $l$  is the coordinate referred along the rod median in the deformed state;  $\lambda$  is the coordinate referred perpendicularly to  $l$ ;  $\theta$  is the rotation of the rod cross-section connected with flexural strain;  $\theta' - \theta$  is the derivative of the  $l$  coordinate;  $\omega$  is the rod cross-section turning angle as a function of shear strain;  $\varepsilon_0$  is the deformation of the centre line passing through the centre of gravity under tension or compression.

The allowance for flexural, shear and tensile-compression strains helps to describe deformation of "short" rods when their length is commensurable with the cross-sectional side length. For an arbitrary cross-sectional shape, the following expressions are valid

$$M = \iint_S \sigma_{ll} \lambda dS, \quad P = \iint_S \sigma_{ll} dS, \quad Q = \iint_S \sigma_{\lambda l} dS. \quad (10)$$

where  $M$  is the bending moment;  $Q$ ,  $P$  are the transverse and longitudinal forces. Therefore, the equilibrium Eqs. for the cantilever rod for the large deflection case will take the form

$$\begin{aligned} Q &= F_y \cos(\theta + \omega) - F_x \sin(\theta + \omega), \\ P &= F_x \cos(\theta + \omega) + F_y \sin(\theta + \omega), \\ M &= F_y (x_L - x) - F_x (y_L - y). \end{aligned} \quad (11)$$

Substituting Eqs. (8) and (9) into (10) gives

$$\begin{aligned}
\omega &= \frac{-k}{G_f S} (F_x \sin(\theta + \omega) - F_y \cos(\theta + \omega)) + \int_0^t R(t - \tau) \omega(\tau) d\tau, \\
\varepsilon_0 &= \frac{1}{E_f S} (F_y \sin(\theta + \omega) + F_x \cos(\theta + \omega)) + \int_0^t R(t - \tau) \varepsilon_0(\tau) d\tau, \\
\theta' &= \frac{1}{E_f J} (F_y (L + \varepsilon_{nm} \xi - x) - F_x (\varepsilon_{nm} \eta - y)) + \int_0^t R(t - \tau) \theta'(\tau) d\tau, \\
x' &= \cos(\theta + \omega), \\
y' &= \sin(\theta + \omega).
\end{aligned} \tag{12}$$

where  $J$ ,  $S$  are the second moments of the area and the cross-sectional area of the rod, correspondingly;  $E_f$  is Young's modulus of rod material;  $k$  is the coefficient complying with non-uniformity of tangential stress distribution over the cross-sectional area. In our calculations we assumed  $k = 1$ .

Therefore, a system of Eqs. was obtained for the five unknown coordinates  $l$  and time functions. Let us apply the following boundary conditions:  $\theta(0, t) = x(0, t) = y(0, t) = 0$ . In (12)  $\eta$ ,  $\xi$  are constants. Solution of these combined Eqs. using the finite difference method allows us to obtain the coordinates of the free end of rod as a function of five variables, viz:

$$\begin{aligned}
x_L &= x(L, t) = f_x(F_x, F_y, \eta, \xi, t), \\
y_L &= y(L, t) = f_y(F_x, F_y, \eta, \xi, t).
\end{aligned} \tag{13}$$

During computation of (12) it was taken into account that the  $l$  coordinate differentiation is made in the deformed state. Therefore, the increment of the  $l$  parameter was assumed equal to  $dl = (1 + \varepsilon_0) \frac{L}{n_0}$ . Here,  $n_0$  is a discretization number. The solution of (12) was carried out for

a specified  $t$ . It should be mentioned that the structure of Rzhanitsyn's relaxation function (7) causes the integral terms in (12) to contain  $\theta$ ,  $\gamma$  and  $\varepsilon_0$  functions which were defined during the previous steps.

The conditions for calculation of the required forces are of the type

$$\begin{cases} f_x(F_x, F_y, \eta, \xi, t) = L + \varepsilon_{nm}(t) \xi, \\ f_y(F_x, F_y, \eta, \xi, t) = \varepsilon_{nm}(t) \eta. \end{cases} \tag{14}$$

The solution of Eqs. (12) and (14) was obtained numerically with the help of MathCad® 7.0 software. The system of nonlinear Eqs. was solved using Newton's method. As the initial approximation we took the solution of the previous step. Therefore, we obtain the functions  $F_x(\eta, \xi, t)$ ,  $F_y(\eta, \xi, t)$  which can be presented as follows

$$\begin{aligned}
F_x &= C_{x1} \xi + C_{x2} \eta + C_{x3} \xi \eta + C_{x4} \xi^2 + C_{x5} \eta^2 + \\
&+ C_{x6} \xi^2 \eta + C_{x7} \xi \eta^2 + C_{x8} \xi^3 + C_{x9} \eta^3 + C_{x10} \xi^2 \eta^2.
\end{aligned} \tag{15}$$

At a given  $t$ , the coefficients  $C_{xj}$ ,  $C_{yj}$  ( $j = 1..10$ ) can be defined by standard regression procedures. The stress tensor components are related through the forces (15) as follows:

$$\begin{aligned}\sigma_{x^0x^0} &= F_{x1} \frac{1}{\pi(L + \varepsilon_{nm}\xi_2)(L + \varepsilon_{nm}\xi_3)}, \\ \sigma_{y^0y^0} &= F_{x2} \frac{1}{\pi(L + \varepsilon_{nm}\xi_1)(L + \varepsilon_{nm}\xi_3)},\end{aligned}\quad (16)$$

$$\begin{aligned}\sigma_{z^0z^0} &= F_{x3} \frac{1}{\pi(L + \varepsilon_{nm}\xi_1)(L + \varepsilon_{nm}\xi_2)}, \\ \sigma_{x^0y^0} &= F_{y1} \frac{1}{\pi(L + \varepsilon_{nm}\xi_2)(L + \varepsilon_{nm}\xi_3)} \frac{\varepsilon_{x^0y^0}}{(\varepsilon_{x^0y^0}^2 + \varepsilon_{x^0z^0}^2)^{1/2}}, \\ \sigma_{x^0z^0} &= F_{y1} \frac{1}{\pi(L + \varepsilon_{nm}\xi_2)(L + \varepsilon_{nm}\xi_3)} \frac{\varepsilon_{x^0z^0}}{(\varepsilon_{x^0y^0}^2 + \varepsilon_{x^0z^0}^2)^{1/2}}, \\ \sigma_{y^0z^0} &= F_{y2} \frac{1}{\pi(L + \varepsilon_{nm}\xi_1)(L + \varepsilon_{nm}\xi_3)} \frac{\varepsilon_{y^0z^0}}{(\varepsilon_{x^0y^0}^2 + \varepsilon_{y^0z^0}^2)^{1/2}}.\end{aligned}\quad (17)$$

The stresses for the XYZ system were then redefined. Because of the chaotic orientation of the unit cells, the stress tensor components should be averaged over direction (Euler's angles)

$$\sigma_{nm} = \int_0^\pi \int_0^{2\pi} \int_0^{2\pi} \sigma_{nm}(\beta_1, \beta_2, \beta_3) \frac{\sin \beta_3}{8\pi^2} d\beta_1 d\beta_2 d\beta_3. \quad (18)$$

Therefore, for the known stress to time dependence, we defined time dependencies of the stresses in a representative volume of the material.

## 5.2 Calculation example: Uniaxial stress

As an example of using above technique, let us examine the stress-strain state of an elastic porous material based on high density polyethylene (HDPE). Experimental data for HDPE were obtained from [Goldman, 1979]:  $G_f = 237$  MPa;  $K_f = 1402$  MPa;  $A = 0.022$  s<sup>-β</sup>;  $\beta = 2.995 \cdot 10^{-5}$  s<sup>-1</sup>;  $\alpha = 0.175$ .

Averaging in all possible loading directions (14) makes the simulated material isotropic at the macroscopic level. The  $\tau(\gamma)$  function therefore characterizes the dependence of stress on strain deviator components  $\tau(\gamma) = s_{nm}(2v_{nm})$ . Thus, if functions  $\tau(\gamma)$  and  $p(\Theta)$  are known, it is possible to simulate isotropic material behaviour at an arbitrary homogeneous stress-strain state. Hence, for a uniaxial stress ( $\sigma_{ZZ} \neq 0$ ) the following relations are true

$$\begin{aligned}2v_{ZZ} &= \frac{4}{3} \varepsilon_{ZZ}(1 + \mu); \\ \Theta &= (1 + \varepsilon_{ZZ})(1 - \varepsilon_{ZZ}\mu)^2 - 1; \\ s_{ZZ} &= \frac{2}{3} \sigma_{ZZ}; \\ \sigma &= \frac{1}{3} \sigma_{ZZ}.\end{aligned}\quad (19)$$

We introduce the transverse strain factor  $\mu = -\frac{\varepsilon_{xx}}{\varepsilon_{zz}}$ , which is analogous to Poisson's ratio in the linear elasticity region. Making allowance for a large bending flexure of the ribs where  $\mu$  depends on strain  $\varepsilon_{zz}$ , this dependence is determined by the following Eq.

$$\tau\left(\frac{4}{3}\varepsilon_{zz}(1+\mu)\right) = 2p\left((1+\varepsilon_{zz})(1-\varepsilon_{zz}\mu)^2 - 1\right). \quad (20)$$

Under stretching,  $\mu$  also decreases rapidly when the strain reaches  $\varepsilon_{cr}$ . In addition, the  $\mu(\varepsilon_{zz})$  dependence rapidly passes on the horizontal plateau  $\mu(\varepsilon_{zz}) = \text{const} = \nu^0$ , where Poisson's ratio  $\nu^0$  is defined as

$$\nu^0 = \frac{3K - 2G^0}{6K + 2G^0}, \quad (21)$$

here  $K$  is the foam bulk modulus defined by the initial part of the  $p(\Theta)$  curve;  $G^0$  is the shear modulus defined by the  $\tau(\gamma)$  curve.

It was found that the  $\mu(\varepsilon_{zz})$  function does not depend on the strain rate. In Figure 14 the dependence of the factor  $\mu$  on the longitudinal strain  $\varepsilon_{zz}$  at stretching (a) and compression (b) of an elastic cellular plastic based on HDPE ( $V_f = 0.01$ ) is presented. Under compression the strain reaches some critical value  $\varepsilon_{cr}$  and  $\mu$  rapidly decreases and becomes negative at  $\varepsilon_{zz} > 0.9\%$ . Such an anomaly of the elastic behaviour was experimentally observed in polymer foams [Lakes, 1987]. Our investigations showed that this effect may occur in cellular materials with a tetrahedronal cell form when the cell ribs buckle inward or in a honeycomb microstructure.

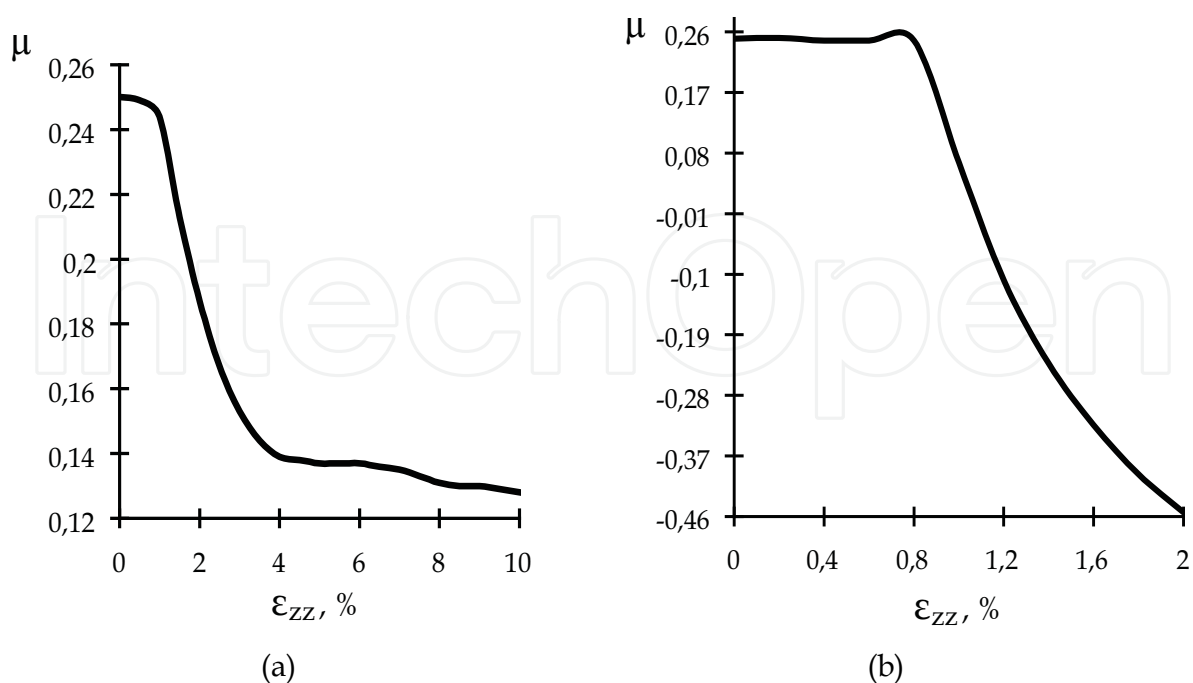


Fig. 14. Dependence of transverse strain factor  $\mu$  on longitudinal strain  $\varepsilon_{zz}$  under stretching (a) and compression (b) of flexible cellular plastics

At small strains,  $\mu$  remains constant and coincides with Poisson's ratio. Under compression the strain reaches some critical value  $\varepsilon_{cr}$  and  $\mu$  rapidly decreases and becomes negative at  $\varepsilon_{ZZ} > 0.9\%$ . Under stretching,  $\mu$  decreases rapidly when the strain reaches  $\varepsilon_{cr}$  and  $\mu(\varepsilon_{ZZ})$  dependence passes on the horizontal plateau.

By defining the  $\mu(\varepsilon_{ZZ})$  function, the dependence of stress  $\sigma_{ZZ}$  on strain  $\varepsilon_{ZZ}$  can be obtained as

$$\sigma_{ZZ}(\varepsilon_{ZZ}) = \frac{3}{2} \tau \left( \frac{4}{3} \varepsilon_{ZZ} [1 + \mu(\varepsilon_{ZZ})] \right). \quad (22)$$

At small strains, stability of  $\mu$  allows us to determine the correlation between  $\varepsilon_{cr}$ ,  $\Theta_{cr}$  and  $\gamma_{cr}$

$$\varepsilon_{cr} = \frac{1}{1 - 2\nu} \Theta_{cr}, \quad \gamma_{cr} = \frac{4(1 + \nu)}{3(1 - 2\nu)} \Theta_{cr}. \quad (23)$$

### 5.3 Comparison with experimental data

To examine the applicability of the theoretical model for foam deformation properties, we compared the calculated and experimental values of the relative Young's modulus  $E/E_f$  and critical strains  $\varepsilon_{cr}$  proceeding from the following considerations: the majority of experimental data on deformation of elastic foams are based on their uniaxial compression behaviour; the calculated stress/strain dependence and the experimental behaviour are almost linear at  $\varepsilon < \varepsilon_{cr}$ . As it was shown in [Hilyard & Cunningham, 1987],  $\sigma_{ZZ}(\varepsilon_{ZZ})$  dependence at  $\varepsilon_{ZZ} > \varepsilon_{cr}$  to a certain degree is conditioned by inhomogeneity of the inner structure of the material.

During definition of Young's modulus  $E$  of an elastic cellular plastic, we considered that the rod cross-section turning angles are small ( $\cos(\theta + \omega) \approx 1$ ,  $\sin(\theta + \omega) \approx 0$ ) and we do not consider rod viscosity. In this case, the solutions can be obtained in the analytical form. For the relative Young's modulus, we have

$$\frac{E}{E_f} = V_f \frac{36 + V_f \pi (7 + 4\nu_f)}{216 + 3V_f \pi (9 + 8\nu_f)}, \quad (24)$$

where  $\nu_f$  is the solid phase Poisson's ratio. In particular, for the elastic polymer material we assume that  $\nu_f = 0.49$ . Equations (10) and (15) yield an approximate expression for the critical strain  $\varepsilon_{cr}$

$$\varepsilon_{cr} = \frac{V_f \pi^3 [72 + V_f \pi (9 + 8\nu_f)]}{72 [36 + V_f \pi (7 + 4\nu_f)]}. \quad (25)$$

The dependence of the relative Young's modulus  $E/E_f$  on the relative solid volume fraction  $V_f$  for the elastic foam is presented in Figure 15.

In Figure 15, curve 1 corresponds to Eqs. (23). Curve 2 agrees with the results obtained in [Warren & Kraynik, 1987]. Curve 3 meets the results obtained in [Beverte & Kregers, 1987] using the semi-axes hypothesis. Curve 4 corresponds to the analytical expression



$$\frac{E}{E_f} = \frac{V_f}{3}(1 - 2\nu') = 0,16V_f, \tag{26}$$

obtained in [Gibson & Ashby, 1982]. Here  $\nu'$  is the Poisson's ratio of the material dependent on the number of rods in structural unit  $N$ . For simulation of mechanical behaviour of the rubber foam [Gibson & Ashby, 1982], we used a structural element with  $4 < N < 8$ , when  $\nu' = 0.26$ . Curve 5 in Figure 15 corresponds to the empirical relation for the relative Young's modulus of foam rubbers [Hilyard & Cunningham, 1987]

$$\frac{E}{E_f} = \frac{V_f}{12}(2 + 7V_f + 3V_f^2). \tag{27}$$

The circles in Figure 15 reflect experimental data for the foam rubber [Lederman, 1971]. This comparison proves that the proposed technique makes it possible to predict quite accurately elastic properties of the material at  $V_f < 0,15$ .

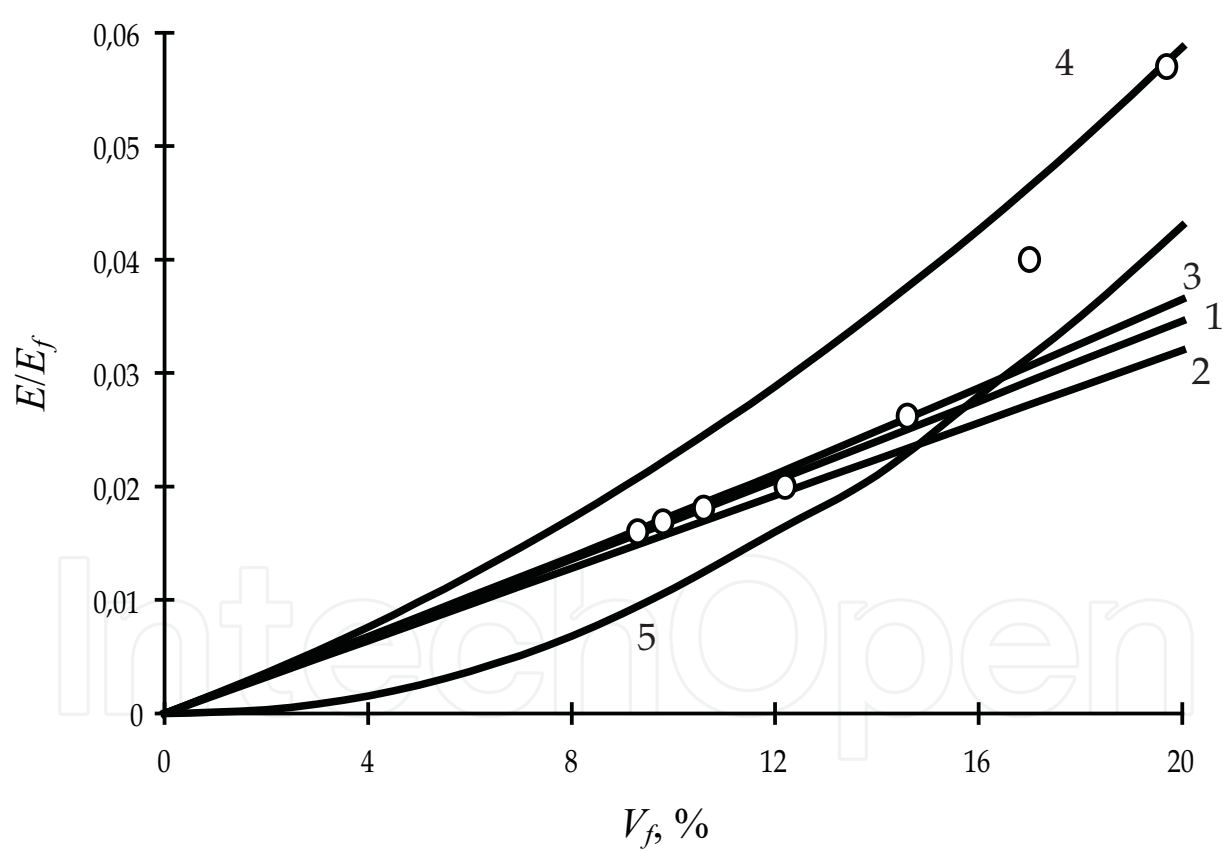


Fig. 15. The dependence of relative Young modulus  $E/E_f$  on the solid phase volumetric fraction  $V_f$  for the flexible foam: curve 1 corresponds to Eqs. (23); curve 2 corresponds to results obtained in [Warren & Kraynik, 1987]; curve 3 corresponds to results obtained in [Beverte & Kregers, 1987]; curve 4 corresponds to results obtained in [Gibson & Ashby, 1982]; curve 5 corresponds to results obtained in [Hilyard & Cunningham, 1987]; circles correspond to experimental data [Lederman, 1971]

5.4 Construction of the mesomechanical model

Mesomechanical (in the scale of the separate cells) description of cellular structure is time-consuming but a very informative method. A possibility for the determination of Poisson’s ratio during special thermomechanical treatment of basic porous material when convex structural cells transform into concave ones as shown in Figure 16, is an advantage of the mesoscopic model.

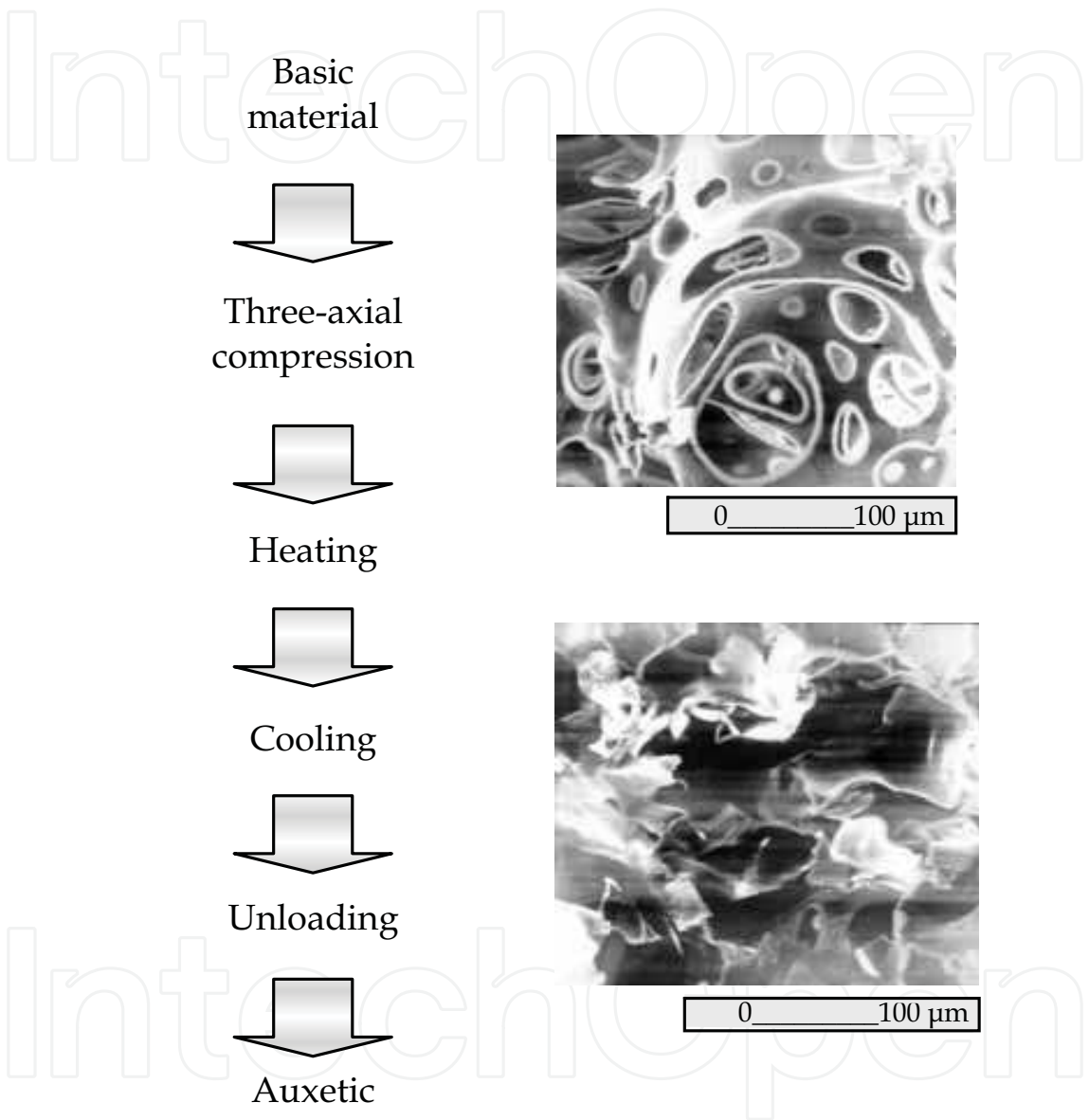


Fig. 16. A scheme of obtaining the auxetic material using transformation of ther basic structure into the inverted one with concave cells. Electron microscopy of a porous polyurethane fragment with magnification 50\*

Previously, the determination of  $\nu$  as a function of the transverse and longitudinal strain was achieved for the case of compression of the sample made of a one-phase material with known values of Poisson’s ratio (Figure 1a). The geometrical sizes of the rectangular sample are  $L_x = 50 \mu\text{m}$ ,  $L_y = 250 \mu\text{m}$ ; the compressive strain is  $\varepsilon_y = 0.5\%$ . The calculated results are shown in Table 5. It should be noted that the technique has an acceptable accuracy which

increases as the friction between the sample and the plates decreases. This fact is explained by a free slip of the contact surfaces.

For calculation of the effective elastic characteristics of the porous material mesofragments we replace the real structure by a system of cells of regular polyhedrons. The transformation of the porous material into the auxetic one appears to be possible at bulk compression  $V_{in}/V_{tr}$  equal to  $1.4\div4.8$  where  $V_{in}$ ,  $V_{tr}$  are the volume of the initial and transformed structure respectively. The best results are achieved at  $V_{in}/V_{tr} = 3.3\div3.7$ . This agrees with the data derived for foamed polyurethane and copper sponge.

The simulation allows us to describe cell transformation at the expense of free volume due to connection of structural units providing the required deformation mode.

The number of node	$u_x, \mu\text{m}$			
	$f = 0.1$		$f = 0.5$	
	Left side	Right side	Left side	Right side
1	-0.0507	0.0498	-0.0510	0.0493
2	-0.0507	0.0498	-0.0510	0.0493
3	-0.0507	0.0498	-0.0510	0.0494
4	-0.0507	0.0498	-0.0509	0.0494
5	-0.0506	0.0499	-0.0508	0.0495
6	-0.0506	0.0499	-0.0508	0.0496
7	-0.0506	0.0500	-0.0507	0.0498
8	-0.0506	0.0503	-0.0508	0.0503
9	-0.0504	0.0483	-0.0504	0.0499
10	-0.0373	0.0370	-0.0471	0.0405
$u_x$ , average	-0.04929	0.04846	-0.05045	0.0487
$u_x$ , total average	0.048875		0.049575	

Table 5. The calculation results of the transverse displacements

5.5 Mesomechanical analysis

According to the mesomechanical approach, some systems of regular polyhedrons, presented in Figure 17, were constructed for calculation of Poisson’s ratio  $\nu$  during structural transformation under compression (Figure 16). In the numerical example, we give the following initial data for the solid phase of the porous material  $E = 1$  GPa,  $\nu = 0.1$ ; the sizes of the fragment  $240\cdot280\text{ }\mu\text{m}$  and the periodic cell  $34\cdot34\text{ }\mu\text{m}$ , the friction coefficient on the contacting surface with the rigid plates is  $f = 0.5$ .

Besides the linear elastic solid phase, we have assumed a physically nonlinear multimodular solid phase. In the last case, the stepwise dependence of Young’s modulus on the stress component has been used (1).

We then simulated deformation of the initial structure with rectangular cells to analyse the formation of auxetic properties under compression of traditional porous material. To increase the accuracy, Poisson’s ratio was determined by averaging the displacements for the left and right sides of the model structure fragment. According to Table 6, the results in the case of a multimodule solid phase seems to be more stable than for  $E = \text{const}$  and at less expressed auxetic properties (stability loss of the porous fragment made of multimodular material is absent at compression displacement  $u_y = 14.0\text{ }\mu\text{m}$ ).

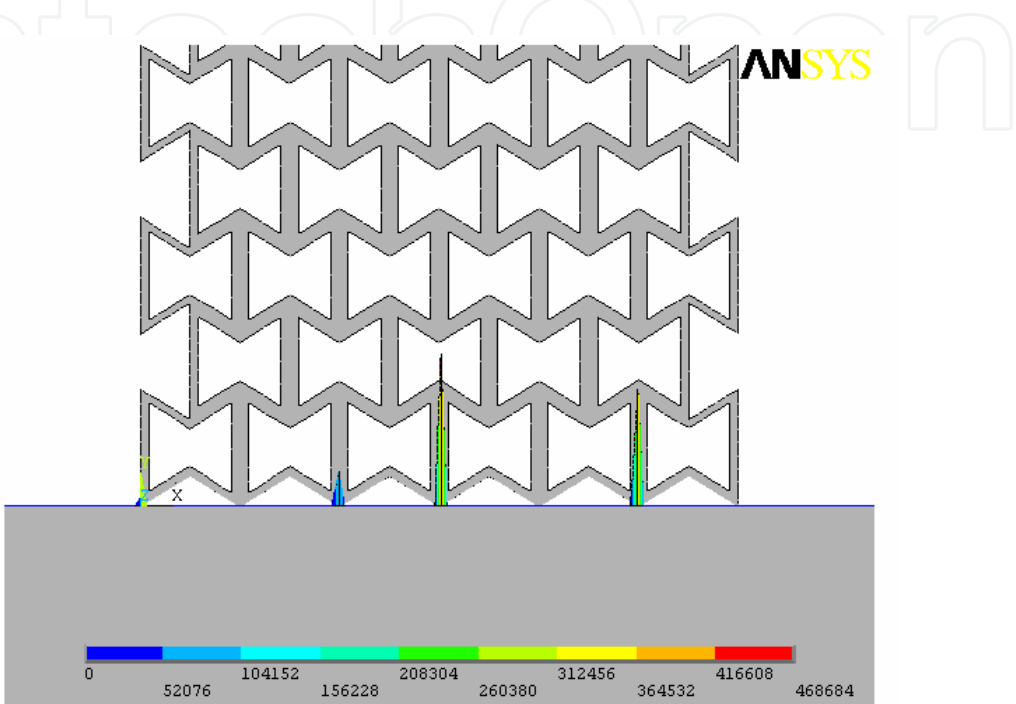


Fig. 17. Distribution of contact pressure under deformation of the porous structure (the vertical compressive displacement  $u_y = 0.1\text{ }\mu\text{m}$ )

$u_y, \mu\text{m}$	1.4	2.8	7.0	14.0*	21.0	28.0	35.0	42.0
$E = \text{const}$	-0.040	-0.054	-0.085	-0.49	-0.180	-0.222	-0.130	-0.291
$E = E(\sigma)$	-0.0146	-0.0195	-0.0340	-0.076	-0.080	-0.100	-0.118	-

\*stability loss of porous material fragment.

Table 6. The calculation results of Poisson’s ratio  $\nu$

The dependences in Figure 18 were shown in a dimensionless form (compression level was taken as a ratio of normal displacements to the height of the porous material fragment  $u_y/b$ ) for comparison under different conditions of loading. It can be seen from Figure 18 that instability of solution is observed at a step-by-step loading of the porous material with hexagonal cells at a deformation level 5%. The porous material with hexagonal cells and multimodule solid phase coincide closely. The solution is not converged for the porous material with square cells at deformation level more than 15% with local unstability in the range 2.5-7.5% and for multimodule solid phase at deformation level more than 10%. The solution is not converged at the deformation level more than 5% for the concave cells with

linear elastic and multimodular solid phase. According to the previous stress history the solution is not converged at the deformation levels greater than 7.5% and 3% for the square and concave cells respectively.

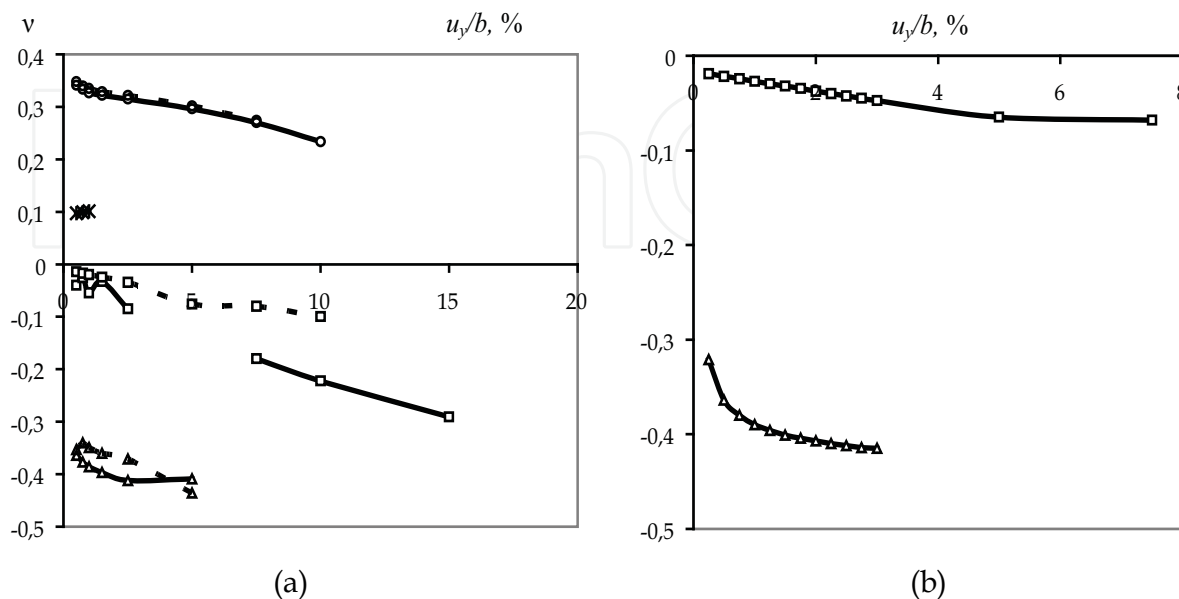


Fig. 18. Dependence of Poisson's ratio on compression level: (a) step-by-step loading; (b) accounting the previous stress history for the porous material with square cells (squares), hexagonal cells (generated angle  $\alpha = 60^\circ$ ) (triangles), circular cells (stars) and with multimodule solid phase (hatches)

The analysis of the stress-strain state of these cellular structures for various deformation levels shows that Poisson's ratio is near to zero at the initial stress state but decreases significantly under compression of the material, which its solid phase has a constant elasticity modulus. The predicted auxetic behaviour is due to generation of the concave cells at the determinative compression level. Poisson's ratio decreases for the structure with the given concave cells transferring into a plateau. At significant deformation, the solution is not converged due to closing of the cell edges.

At the macroscale the model of the cell structure is unstable. This may result in the a displacement of the fragment (in the given example this takes place at compression level  $u_y = 14 \mu\text{m}$ ). For obtaining a stable solution, it is necessary to take into consideration the previous stress history of the contact friction process (Fig. 18b). The account of the previous stress history is also important for calculating the auxetic self-lock mode at the conditions of contact compression and shear [Shilko et al, 2008a].

### 5.6 Prediction of auxetic effects in porous materials with nano-sized cells

Self-assembling high-strength and rigid materials of small density are of great interest like Langmuir films. This may be reached by the auxetic porous material "construction" on the micro- and nano-size level. It is important that the value of adhesion forces  $F$  increases essentially at decreasing of the gap  $H$  between solid surfaces. The values of the adhesion force are shown in Table 3 for two pairs of polymers and three values of the gap  $H$  according to

$$F = \frac{A_{12}}{6\pi H^3},$$

(28)

where  $A_{12}$  is the Hamaher constant and  $H$  is the distance between surfaces. It is seen that a sharp increase of the adhesion force takes place in nano-sized cells of the porous material.

Material	F, MPa			A <sub>12</sub> , Erg
	H = 10A	H = 5A	H = 4A	
Polytetrafluorethylene - Polyimide	7.38	51.1	115.3	1.39*10 <sup>-12</sup>
Polycaproamide - Polycaproamide	7.30	58.3	113.9	1.37*10 <sup>-12</sup>

Table 3. Estimation of adhesion forces in nano-sized cells on the basis of polymers

The calculations of the deformed state of the porous material subject to adhesion forces and multimodule effect simultaneously, show a possibility of self-assembling of a spontaneous, energetically preferable auxetic nano-sized structure as shown in Figure 19. So, the auxetic porous materials with micro- and nano-sized cells, having good combination of density, deformational and strength properties, seem quite preferable for many technical and biomedical applications. Analytical and numerical modelling describes the cellular solid transformation resulting in microbuckling of the cell walls under certain loading conditions and providing the auxetic deformation mode. Geometrically simple mesomechanical models of the porous material based on cubic, rectangular and concave structural units have been investigated in the present paper taking into account such important factors as large strains, history of loading, physical nonlinearities of solid phase, adhesive interaction and so on. The limitations of the effective finite element simulation are caused by stability loss of the representative fragment of structure. The possibility of compression-driven self-assembly of nano-sized auxetics due to the increasing adhesion force between the cell walls has been predicted.

6. Conclusion

- The systematic analysis of the problem of developing adaptive composites has enabled us to trace evolution of structural organization of artificial materials, to clarify the mechanisms of adaptation to the external action, and to disclose, to a certain degree, the effect of structure on formation of the optimum back reaction.
- In above considered examples of composites, description of adaptive structures is formulated as a problem on localizing moving interfaces. The study of synergetic phenomena in the nonliving nature and analogous processes in biological objects will, in our opinion, provide a possibility to find structural-and-functional prototypes of adaptive composites.
- The proposed analytical and numerical models predict self-reinforcing in composites and joints made of auxetics under loading. The role of friction, previous stress history,

multimodule solid phase and adhesion forces acting between the walls of cells were shown in the formation of auxetic properties of the porous materials as the composites with the gas phase.

- The limiting values of compression deformation on the stability criterion of cellular structures under compression and the possibility of energetically preferable self-assembly of auxetic porous nano-sized materials have been predicted.
- It's seemed that realization of self-healing in composites made of auxetic and multimodule materials is a perspective goal of further studies.

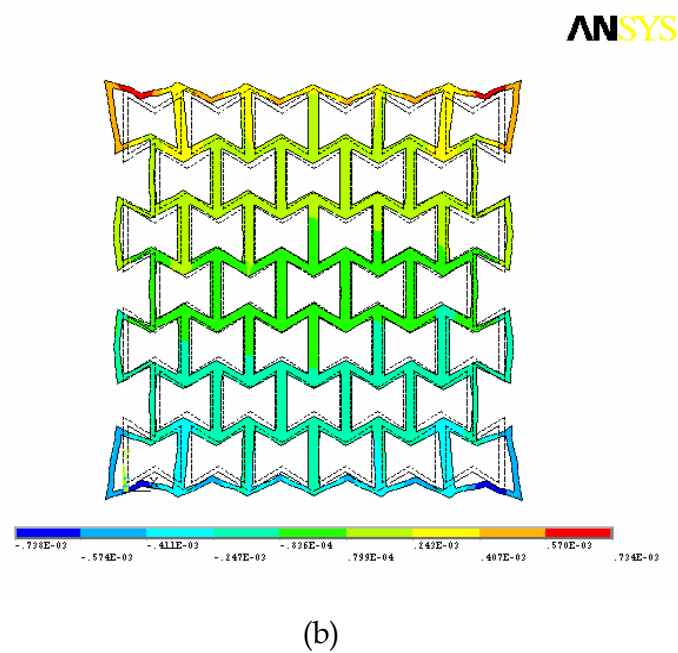
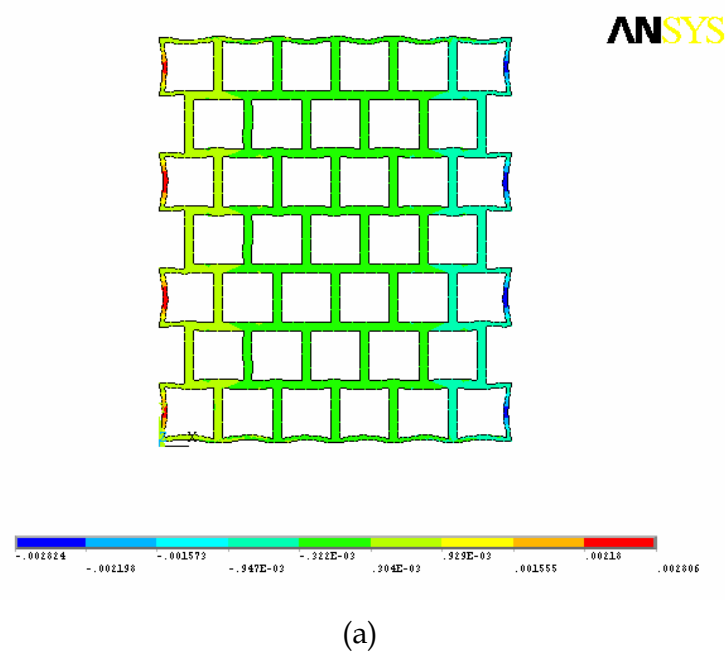


Fig. 19. Deformation modes of the porous material with initially rectangular (a) and concave (b) shape of the cells under the action of adhesion forces



## 7. Acknowledgement

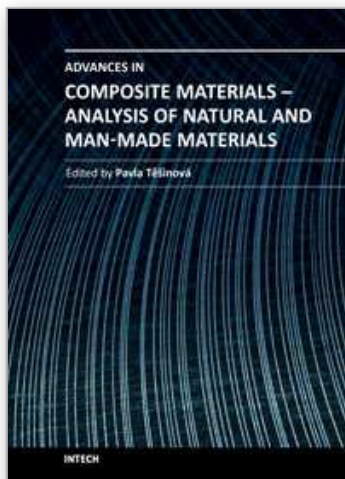
The author is grateful for assistance to Prof. Yu. Pleskachevsky, Prof. R.D. Adams, Dr. D. Chernous and K. Petrokovets.

## 8. References

- Anfinogenov, S.B. Kurek, M.F. Shilko, & S.V. Chernous, D.A. (2008). Mechanical and frictional properties of biological elastomers: Part 1: Description of human skin relaxation under tension. *Russian Journal of Biomechanics*, Vol. 12, No. 3, pp. 42–48, ISSN 1812-5123.
- Baughman, R.H. Galvao, D.S. (1993). Crystalline networks with unusual predicted mechanical and thermal properties. *Nature*, Vol. 365, pp. 735-737, ISSN 028-0836.
- Bell, J.F. (1968). The physics of large deformation of crystalline solids. Springer tracts in natural philosophy. Vol. 14, Springer, Berlin-Heidelberg-New York.
- Bergman, D.J. Inan, E. (Ed(s)). (2004). Continuum models and discrete systems, Kluwer Academic Publishers, ISBN 1-4020-2314-6, Dordrecht-Boston-London.
- Beverte, I.V., Kregers, A.F. (1987), *Mechanics of Composite Materials*. Vol. 23, No. 1, pp. 27–33).
- Chernous, D.A. Shilko, S.V. Konyok, D.A. & Pleskachevsky Yu.M. (2003). Nonlinear viscoelastic behavior of flexible cellular plastics: refined rod model. *International Journal of Applied Mechanics and Engineering*, No. 1, pp. 27-41, ISSN 1425-1655.
- Galaev, Yu.I. (1995). Smart polymers in biotechnology and medicine. *Russian Chemical Reviews*, Vol. 64, No. 5, pp. 505-524, ISSN 0036-021X.
- Gibson, L.J. Ashby, M.F. (1982). The mechanics of three-dimensional cellular materials. *Proceedings of the Royal Society A*, Vol. 382, No. 3, pp. 43-59, ISSN 1364-5021.
- Goldman, A.Ya. (1979). Strength of constructional plastics, *Mashinostroenie*, Leningrad (in Russian).
- Hilyard, N.C. Cunningham, A. (1987). Low Density Cellular Plastics: Physical Basis of Behaviour, Chapman and Hall, London.
- Hirotsu, S. (1991). Softening of bulk modulus and negative Poisson's ratio near the volume phase transition in polymer gels. *Journal of Chemical Physics*, Vol. 94, No. 5, pp. 3949-3957, ISSN 021-9606.
- Kolupaev, B.S. Lipatov, Yu.S. Nikitchuk, V.I. Bordyuk, N.A. & Voloshin, O.M. (1996). Composite materials with negative Poisson coefficient. *Journal of Engineering Physics and Thermophysics*, Vol. 69, No. 5, pp. 542-549, ISSN 1062-0125.
- Koniok, D.A. Voitsekhovskiy, K.V. Pleskachevsky, Yu.M. & Shilko, S.V. (2004). Materials with negative Poisson's ratio. (The review). *Journal on Composite Mechanics and Design*, Vol. 10, No. 1, pp. 35-69, ISSN 1682-3532.
- Lakes, R. (1987). Foam structure with a negative Poisson's ratio. *Science*, Vol. 235, pp. 1038-1040, ISSN 0036-8075.
- Landau, L.D. Lifshitz, E.M. (1986). *Theory of Elasticity*. Vol. 7 (3rd ed.), Butterworth-Heinemann, ISBN 978-0-750-62633-0, Oxford.
- Lederman, J.M. (1971). The prediction of the tensile properties of flexible foams. *Journal of Applied Polymer Science*, Vol. 15, No. 3, pp. 693-703, ISSN 0021-8995.

- Prigogine, I. Stengers, I. (1984). *Order out of Chaos: Man's new dialogue with nature*, Flamingo, ISBN 0006541151, London.
- Schwartz, M. (2007). *Encyclopedia of Smart Materials*, John Wiley & Sons, Inc. ISBN 0-471-17780-6, New York.
- Shilko, S.V. Stolyarov, A.I. (1996). Friction of anomalously elastic bodies. Negative Poisson's ratio. Part 2. Calculation of self-locking parameters. *Journal of Friction and Wear*, Vol. 17, No. 4, pp. 23-29, ISSN 0202-4977.
- Shilko, S.V. Petrokovets, E.M. & Pleskachevsky, Yu.M. (2008). Peculiarities of friction in auxetic composites. *Physica status solidi B*, Vol. 245, No. 3, pp. 591-597, ISSN 0370-1972.
- Shilko, S.V. Petrokovets, E.M. & Pleskachevsky, Yu.M. (2008). Prediction of auxetic phenomena in nanoporomaterials. *Physica status solidi B*, Vol. 245, No. 11, pp. 2445-2453, ISSN 0370-1972.
- Warren, W.E. Kraynik, A.M. (1987). *The Winter Annual Meeting of the ASME*, Boston, pp. 123-145.
- Wei, G. Edwards, S.F. (1999). Effective elastic properties of composites of ellipsoids (II). Nearly disc- and needle-like inclusions. *Physica A*, Vol. 264, pp. 404-423, ISSN 0378-4371.
- Wojciechowski, K. Alderson, A. Alderson, K.L. Maruszewski, B. & Scarpa, F. (2007). Preface. *Physica status solidi B*, Vol. 244, No. 3, pp. 813-816, ISSN 0370-1972.

IntechOpen



## **Advances in Composite Materials - Analysis of Natural and Man-Made Materials**

Edited by Dr. Pavla Tesinova

ISBN 978-953-307-449-8

Hard cover, 572 pages

**Publisher** InTech

**Published online** 09, September, 2011

**Published in print edition** September, 2011

Composites are made up of constituent materials with high engineering potential. This potential is wide as wide is the variation of materials and structure constructions when new updates are invented every day. Technological advances in composite field are included in the equipment surrounding us daily; our lives are becoming safer, hand in hand with economical and ecological advantages. This book collects original studies concerning composite materials, their properties and testing from various points of view. Chapters are divided into groups according to their main aim. Material properties are described in innovative way either for standard components as glass, epoxy, carbon, etc. or biomaterials and natural sources materials as ramie, bone, wood, etc. Manufacturing processes are represented by moulding methods; lamination process includes monitoring during process. Innovative testing procedures are described in electrochemistry, pulse velocity, fracture toughness in macro-micro mechanical behaviour and more.

### **How to reference**

In order to correctly reference this scholarly work, feel free to copy and paste the following:

Shilko Serge (2011). Adaptive Composite Materials: Bionics Principles, Abnormal Elasticity, Moving Interfaces, Advances in Composite Materials - Analysis of Natural and Man-Made Materials, Dr. Pavla Tesinova (Ed.), ISBN: 978-953-307-449-8, InTech, Available from: <http://www.intechopen.com/books/advances-in-composite-materials-analysis-of-natural-and-man-made-materials/adaptive-composite-materials-bionics-principles-abnormal-elasticity-moving-interfaces>

**INTECH**  
open science | open minds

### **InTech Europe**

University Campus STeP Ri  
Slavka Krautzeka 83/A  
51000 Rijeka, Croatia  
Phone: +385 (51) 770 447  
Fax: +385 (51) 686 166  
[www.intechopen.com](http://www.intechopen.com)

### **InTech China**

Unit 405, Office Block, Hotel Equatorial Shanghai  
No.65, Yan An Road (West), Shanghai, 200040, China  
中国上海市延安西路65号上海国际贵都大饭店办公楼405单元  
Phone: +86-21-62489820  
Fax: +86-21-62489821

© 2011 The Author(s). Licensee IntechOpen. This chapter is distributed under the terms of the [Creative Commons Attribution-NonCommercial-ShareAlike-3.0 License](https://creativecommons.org/licenses/by-nc-sa/3.0/), which permits use, distribution and reproduction for non-commercial purposes, provided the original is properly cited and derivative works building on this content are distributed under the same license.

IntechOpen

IntechOpen